

01 Aug 2024

Tellurium Enrichment in Copper Tailings: A Mineralogical and Processing Study

José L. Corchado-Albelo

Lana Alagha

Missouri University of Science and Technology, alaghal@mst.edu

Follow this and additional works at: https://scholarsmine.mst.edu/min_nuceng_facwork

 Part of the [Mining Engineering Commons](#)

Recommended Citation

J. L. Corchado-Albelo and L. Alagha, "Tellurium Enrichment in Copper Tailings: A Mineralogical and Processing Study," *Minerals*, vol. 14, no. 8, article no. 761, MDPI, Aug 2024.

The definitive version is available at <https://doi.org/10.3390/min14080761>




This work is licensed under a [Creative Commons Attribution 4.0 License](#).

This Article - Journal is brought to you for free and open access by Scholars' Mine. It has been accepted for inclusion in Mining Engineering Faculty Research & Creative Works by an authorized administrator of Scholars' Mine. This work is protected by U. S. Copyright Law. Unauthorized use including reproduction for redistribution requires the permission of the copyright holder. For more information, please contact scholarsmine@mst.edu.

Article

Tellurium Enrichment in Copper Tailings: A Mineralogical and Processing Study

José L. Corchado-Albelo ^{1,*}  and Lana Alagha ^{1,2,*}¹ Department of Mining and Explosives Engineering, Missouri University of Science and Technology, Rolla, MO 65409, USA² Missouri S&T Research Center for Critical Minerals Research and Engineering, Missouri University of Science and Technology, Rolla, MO 65409, USA

* Correspondence: jlc53w@mst.edu (J.L.C.-A.); alaghal@mst.edu (L.A.); Tel.: +1-(573)-341-7736 (J.L.C.-A.); +1-(573)-341-6287 (L.A.)

Abstract: As the global demand for tellurium (Te) increases, it is crucial to develop efficient recovery methods that consider existing supply streams. This research combines gravity separation and froth flotation processes to enhance the recovery of Te minerals from tailings produced during the beneficiation of copper porphyry ores. Prior to processing, a systematic and comprehensive characterization study of copper tailing (CT) samples was conducted to examine the deportment of Te minerals in different mineral phases and to understand their locking and liberation behavior. Characterization techniques included inductively coupled plasma mass spectrometry (ICP-MS) and TESCAN's integrated mineral analysis (TIMA). Copper tailing characterization showed that minerals with gold (Au), silver (Ag), bismuth (Bi), and Te were present in various forms, including native Au, electrum, tellurides, and sulfosalts. TIMA revealed that >90% of these minerals were primarily hosted in pyrite as less than 10 µm inclusions in the CT. TIMA also revealed that Te minerals exhibited fine-grained liberation of less than 20 µm. Moreover, TIMA results showed that >80% of mica and other silicate minerals were concentrated in size fractions < 38 µm, suggesting that desliming processes would positively impact Te enrichment. The results from the processing tests showed a Te recovery rate of ~77% and a Te enrichment ratio of 13 when using the combination of gravity separation and froth flotation at 90 g/t xanthate collector and 50 g/t glycol frother. The findings from this study show a significant potential for Te recovery from unconventional sources if appropriate physical beneficiation approaches are adopted.

Keywords: critical minerals; pyrite; copper tailing; froth flotation; Cd-Te solar cells

Citation: Corchado-Albelo, J.L.; Alagha, L. Tellurium Enrichment in Copper Tailings: A Mineralogical and Processing Study. *Minerals* **2024**, *14*, 761. <https://doi.org/10.3390/min14080761>

Academic Editor: Wengang Liu

Received: 18 June 2024

Revised: 16 July 2024

Accepted: 21 July 2024

Published: 27 July 2024



Copyright: © 2024 by the authors. Licensee MDPI, Basel, Switzerland. This article is an open access article distributed under the terms and conditions of the Creative Commons Attribution (CC BY) license (<https://creativecommons.org/licenses/by/4.0/>).

1. Introduction

Critical minerals are of paramount concern to both governments and the private sectors due to their strategic importance and potential impact on supply chains [1–3]. Since the early 2010s, there has been renewed interest in these minerals, driven by geopolitical risks, supply chain vulnerabilities, trade exposures, and economic dependencies associated with these specialized commodities [4–6]. The global shift from fossil fuels to more sustainable energy technologies has further underscored the importance of securing ethically sourced and supplied critical minerals [7,8]. This shift has prompted many governments and corporations to classify certain elements or commodities as critical minerals [3,9].

Tellurium (Te) is classified as a critical element by several governments, including the USA, Canada, the United Kingdom, Japan, and India, due to its significance to clean energy transition approaches [10,11]. Despite this key role, Te is one of the rarest elements in nature, with average crustal concentrations of only 3 parts per billion (ppb), which is similar to gold (Au) and platinum group elements (PGEs) [12–15]. This scarcity presents significant challenges in identifying specific Te-enriched deposits. Tellurium is often found

in magmatic nickel–copper (Ni–Cu) sulfide deposits, porphyry copper deposits, and epithermal gold deposits, where it exists in both discrete mineral forms and as inclusions within sulfide minerals like pyrite and chalcopyrite [14,16–18]. Notable Te-rich deposits include the Dachuigou deposit in China, where high-grade ores are up to 25 wt.% Te, and various porphyry copper deposits in the world, such as the Bingham Canyon deposit in the USA [16,18–20]. Common Te minerals include gold tellurides, like calaverite (AuTe_2), sylvanite ($(\text{Au,Ag})\text{Te}_2$), and petzite (Ag_3AuTe_2), as well as bismuth tellurides, such as tetradymite ($\text{Bi}_2\text{Te}_2\text{S}$), and lead tellurides, like altaite (PbTe) [21,22].

In recent years, Te demand has risen due to its increased incorporation into various specialized applications, including metal alloys, glass optical fibers, ceramics, pigments, catalysts, magnetic discs, and solar panels [15,23]. The transition toward sustainable energy sources has highlighted Te's significance as a key element in the production of CdTe thin-film solar photovoltaics (PVs) [24]. Forecasts indicate that 40% of global Te production will cater to CdTe thin-film solar PVs, with the demand expected to rise significantly by 2025 and 2035 [25]. As the solar PV market continues to grow, there is a greater risk of a shortage in Te supply. This highlights the importance of implementing sustainable and resilient supply chain management strategies.

From an economic standpoint, Te is predominantly obtained from copper porphyry deposits using intricate production methods that focus on downstream metallurgical processes [13,14,18]. From 2000 to 2020, approximately 90% of global Te production has been sourced as a by-product of reprocessing copper porphyry deposit anode slimes during refining (Figure 1) [15,18]. However, it has been recently reported that almost 90% of Te contained in the CP ores is deported to the tailings during the early stages of the ore beneficiation process [2,18,26]. The deportment of Te minerals and associated mineral phases to tailing could be due to these minerals being less floatable, locked in gangue minerals, or depressed in early flotation stages [2,18,26].

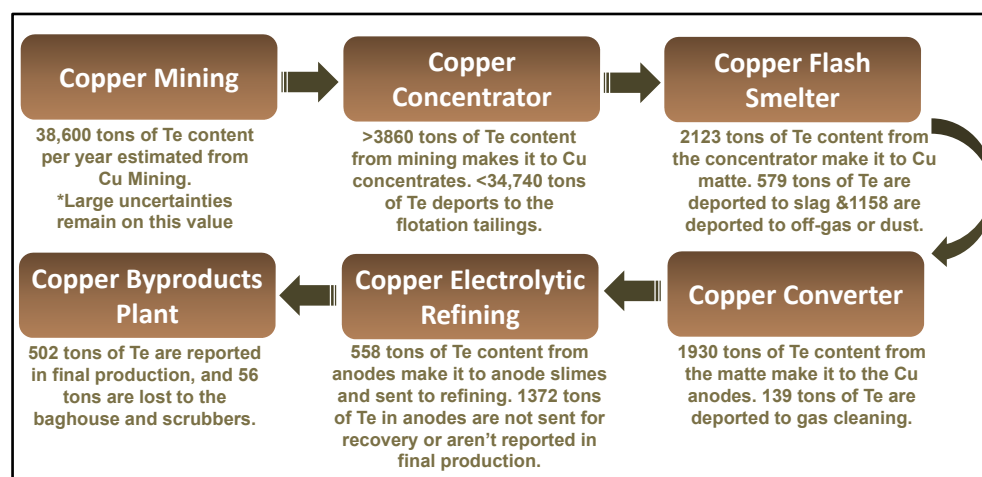


Figure 1. Tellurium production estimates in tons through the copper porphyry processing streams. The Te estimates were based on the world's total production of copper. Modified from [2].

There is limited literature on the behavior of Te minerals in various geologic environments in terms of mineral associations, liberation, and weathering in mine waste streams. For instance, Yano (2013) studied the mode of occurrence of Te in copper porphyry deposits and suggested that Te concentration follows the Au–Ag–Bi–Se–Pb concentrations for bornite and chalcopyrite [16]. Hayes and Ramos (2019) researched the surface chemistry of mine tailings in different weathering environments and highlighted that Te is associated with iron (oxy)hydroxides that could facilitate its mobility and leachability [27]. A recent study by Corchado et al. (2023) showed a case study for a North American copper mining operation, where up to 88% of Te minerals in the flotation feed are lost to flotation tailings.

These minerals are often locked within larger pyrite grains and associated with valuable Au-Ag-Bi minerals [28].

Although a number of studies have explored the recovery of critical minerals from tailing streams [29–32], there is a significant lack of comprehensive research focusing on the recovery of Te from tailings produced during copper processing [26]. This study explored potential beneficiation processes, including gravity separation and froth flotation, to recover Te minerals from CT. To optimize the reagent chemistry, baseline froth flotation experiments were conducted where different reagent chemistries were tested to enhance Te enrichment. Detailed characterization and mineralogical studies were performed on CT feed and products of the physical separation studies using inductively coupled plasma mass spectrometry (ICP-MS) and TESCAN's integrated mineral analysis (TIMA) to precisely identify and quantify Te and the associated valuable minerals. This was crucial to gain detailed insights into the elemental and phase-specific mineral distribution to enable the design of appropriate recovery routes.

2. Materials

2.1. Copper Tailing Samples

The copper tailing (CT) samples were collected from rougher flotation tailings at a major copper producer in the USA. Two sample batches were provided with a time difference of two years; the first batch received was called Tailings 1 (CT1), and the second batch was called Tailings 2 (CT2). As shown in the following section, the two types differed in terms of elemental assay values; however, they had a similar mineralogy. The samples were air-dried and subsequently divided into representative portions for mineralogical and chemical characterizations.

2.2. Flotation Reagent

A conventional flotation collector for froth flotation, sodium isopropyl xanthate (SIPX), was obtained from Fisher Scientific, USA. The thiocarbamate-based collector, EXP300422, was obtained from NeoSolutions (Beaver, PA, USA). The conventional frother, methyl isobutyl carbinol (MIBC), was purchased from Fisher Scientific (Hampton, NH, USA). The glycol-based frother, OREPREP X-237, was obtained from Solvay LLC (East St Louis, IL, USA), also known as Syensqo, as of December 2023. Stock solutions for the collector and frother were prepared at 1 g/L. pH modifiers, including sodium hydroxide (NaOH) and hydrochloric acid (HCl), were purchased from Fisher Scientific, USA and were prepared at 10 g/L and 9.12 g/L stock solutions, respectively.

3. Methodology

3.1. Analysis and Characterization Studies

3.1.1. Inductively Coupled Plasma Mass Spectrometry (ICP-MS)

Inductively coupled plasma mass spectrometry (ICP-MS) from ActLabs (Ancaster, Ontario, CA, USA) was used to accurately quantify Te and other elements in the CT, flotation concentrates, flotation tailings, GS concentrates, GS middling, and GS tailing samples. The ICP-MS “total” digestion process was employed to dry-test powdered mineral samples. This was performed using a four-step dilution process, starting with hydrochloric acid, then nitric acid, perchloric acid, and hydrofluoric acid. The digestion yielded a stable ionic solution used for ICP-MS analysis. Details of procedures used for ICP-MS are reported elsewhere [33].

3.1.2. TESCAN'S Integrated Mineral Analysis

Automated mineralogical analysis was conducted using TESCAN's integrated mineral analysis (TIMA) using a TESCAN MIRA 3 GMU (TESCAN, Warrendale, PA, USA) on CT samples to identify different Te mineral phases and their locking behavior. Data analysis was conducted using TIMA software that utilized different acquisition modes to generate a variety of measurement analyses. This includes four X-ray analysis scanning modes,

namely high-resolution mapping, point spectrometry, line mapping, and dot mapping. Each mode can be further customized to suit specific tasks. To prepare for the TIMA, the materials were sieved into size fractions of +150 μm , +75 μm , +38 μm , and −38 μm , mounted onto an epoxy, ground, and polished to a 0.3 μm alumina powder finish. The samples were coated with carbon to ensure electron conductivity and scanned using a scanning electron microscope (SEM) equipped with energy-dispersive X-ray spectroscopy (EDS) and backscatter electron (BSE) imaging detectors. A watershed transform algorithm analysis was applied with variation in the BSE image and EDS spectra between adjacent pixels to differentiate mineral phases. Mineral identification was carried out using spectral identification protocols based on phase-specific X-ray profiles and elemental intensity selection rules for qualitative mineral identification. Additionally, surface area data and density for individual phases were used to quantify the results [34].

Additionally, bright-phase analysis was used to identify and quantify minerals containing elements of interest, such as gold (Au), silver (Ag), and tellurium (Te), within a sample. The analysis was conducted based on the mean atomic number (MAN) of the minerals, with higher MAN minerals appearing brighter in BSE images. To exclude common sulfides like pyrite, the brightness threshold was set at 60% on a scale of 1 to 100% using a platinum standard, ensuring that only particles containing high-MAN minerals were analyzed. If a high-MAN mineral was part of a larger particle, the entire particle (e.g., silicates and sulfides) was included in the analysis. The TIMA bright-phase analysis did not provide a comprehensive overview of the sample's overall mineralogy, but offered valuable insights into the distribution and occurrence of specific high-MAN minerals. The results were particularly useful for comparing samples with similar mineral compositions and for locating specific minerals within the samples. The minerals identified during bright-phase analysis include native gold, electrum, and Te phases such as tetradymite, altaite, and petzite [34]. TIMA experiments were performed at Montana Technological University's Center for Advanced Materials Processing (CAMP).

3.2. Physical Separation Studies of Copper Tailings

3.2.1. Gravity Separation Studies

Characterization results and preliminary flotation studies indicated that the CT sample had a significant amount of fine particles (slimes) that were mainly composed of micas and other silicates. These slimes were entrained into the froth layer during the flotation process and negatively impacted the concentrate grade [28,32]. Therefore, gravity separation was selected as a method for desliming CT due to its effectiveness in separating fines and recovering valuable, higher-density sulfide minerals. Studies have shown that gravity separation techniques, such as using the Wilfley Table (Metso/Outotec, Helsinki, Finland) can significantly enhance the preconcentration of minerals by creating three distinct streams: concentrate, middlings, and tailings [35,36]. Additionally, gravity separation has been found to be more environmentally sustainable compared to other methods, aligning with the goals of sustainable production of Te [37,38]. In this set of experiments, the Wilfley Table was used for gravity separation (GS) using Tailings 2. Experiments were conducted as a function of the solid-to-liquid ratio (S:L). Three different S:L ratios were selected, 1:15, 1:10, and 1:5, while the remaining GS parameters were consistent at an 11 cm stroke, 0° tilt (flat), slurry flow of 1.2 L/minute, and wash water flow of 1 L/minute [38–41]. The concentrate, middling, and tailing products were dried, weighed, and assayed using ICP-MS. Mass balance (Equation (1)) and recovery (Equation (2)) formulas were used to determine the recovery for Te, Au, Ag, Fe, Cu, and S.

$$Ff = Cc + Mm + Tt \quad (1)$$

In Equation (1), “F” is the mass of the feed/head, “f” is the grade of valuable element or compound in the feed/head, “C” is the mass of the concentrates, “c” is the grade of valuable element or compound in the concentrates, “M” is the mass of the middlings, “m”

is the grade of valuable element or compound in the middlings, = “T” is the mass of the tailings, and “t” is the grade of valuable element or compound in the tailings.

$$R(\% \text{ element or compound}) = \frac{S_s}{F_f} \times 100 \quad (2)$$

In Equation (2), “R” is the recovery of the element or compound, “S” is the mass of the process stream under consideration (C, M, or T), “s” is the grade of valuable element or compound in the process stream under consideration, “F” is the mass of the feed/head, and “f” is the grade of valuable element or compound in the feed/head. Calculations of recovery and enrichment were based on CT-specific grades.

Gravity separation experiments helped establish the distribution and concentration of Te, Au, Ag, Fe, Cu, and S in different GS streams, which were then enriched through targeted flotation strategies.

3.2.2. Froth Flotation Studies

Bench flotation experiments were performed using the Denver D12 flotation machine (Denver Equipment Company, Denver, CO, USA) with a 1 L cell and a 2–7/8 in diameter impeller to establish a baseline for the concentration of Te minerals and their hosts.

The first set of flotation experiments was conducted to select the optimum collector chemistry. Two different collector types were tested using the conditions presented in Table 1. The flotation feed (as received CT) was prepared in tap water at 30 wt.% solids. The slurry was agitated at 900 RPM, and the pH was adjusted to pH 8 using NaOH for 2 min. Then, it was mixed for 3 min after the collector’s addition to the slurry. MIBC was used as a frother at 50 g/t and conditioned for 1 min. The airflow rate was set at 5 L/min. The collector-type selection was informed by Yang et al.’s (2019) findings showing that carbamate and xanthate collectors efficiently recover Te minerals from refractory gold ores [42].

Table 1. List of reagents used as collectors in Te mineral flotation studies of CT.

Reagent Type and Dosage	As-Received CT
EXP300422 (90 g/t) and MIBC (50 g/t)	Tailings 1
SIPX (90 g/t) and MIBC (50 g/t)	
EXP300422 (90 g/t) and OREPREG X-237 (50 g/t)	
SIPX (90 g/t) and OREPREG X-237 (50 g/t)	

Concentrates were collected over 5 min of flotation time. The concentrate and tailing products were dried, weighed, and assayed using ICP-MS. Recovery rates for Te, Au, Ag, Fe, Cu, and S were calculated using Equation (2). These elements were selected as representatives for the valuable Te minerals and their sulfide host minerals based on studies by Yano (2013) and Corchado-Albelo and Alagha (2013), which showed a strong correlation between Te and Au-Ag-Fe-Cu-S in copper porphyry processing streams [16,28].

$$\text{Flotation Enrichment (unitless)} = \frac{c}{f} \quad (3)$$

In the second set of experiments, the effect of the frother type was examined. These experiments followed the same flotation procedures used to test the collector type. Table 1 shows the list of frothers used in this study.

The third set of experiments was carried out using the middling and concentrate streams of GS (i.e., higher-density products) produced at different S:L ratios as flotation feed. These flotation experiments were conducted using the optimum collectors/frother combination identified in the first set of flotation experiments. The concentrate and tailing products were dried, weighed, and assayed using ICP-MS. Recovery was calculated using

Equation (2), and flotation enrichment was calculated using Equation (3). The flotation products with the highest Te enrichment were analyzed using TIMA to gain insights into the deportment of Te minerals after processing and their locking and liberation behavior. Figure 2 shows the strategy used in this work for Te enrichment.

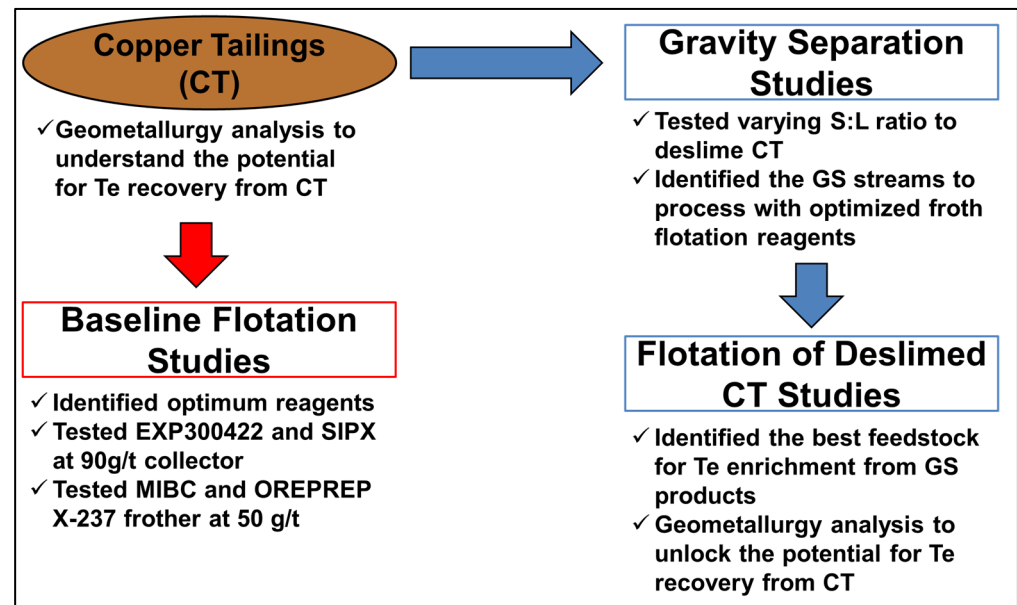


Figure 2. Flowsheet diagram showing the different approaches used in this study for Te enrichment. Baseline flotation tests follow the path of the red arrows and outlined boxes, while the path for desliming followed by optimized flotation are shown with blue arrows and outlined boxes.

4. Results

4.1. Characterization of Copper Tailings

4.1.1. ICP-MS Studies

ICP-MS was used to determine the average concentration of Te, Au, Ag, Fe, and other elements in the as-received CT (Table 2). The term “elements of interest” was assigned to commodities of interest, such as Te, Au, Ag, and Fe, or any elements that interfere with the beneficiation process or elements that are part of multiple critical elements lists worldwide [25,26,43]. The average grades for Te, Au, and Fe in CT samples were 0.40 ppm, 104 ppb, and 3.33%, respectively.

Table 2. Elemental analysis of CT samples determined by ICP-MS.

Elements of Interest	^a Tailings 1 (CT1)	^b Tailings 2 (CT2)	* Tailings Average	Units
Te	0.7	0.3	0.5	ppm
Au	88	165	126.5	ppb
Ag	0.77	0.68	0.725	ppm
Cu	377	860	618.5	ppm
Mo	24.8	91.8	58.3	ppm
Pb	34.8	29.4	32.1	ppm
Ni	<0.5	41	20.75	ppm
Zn	48.3	39.2	43.75	ppm
S	1.81	0.8	1.305	%
As	14.8	8.9	11.85	ppm

Table 2. Cont.

Elements of Interest	^a Tailings 1 (CT1)	^b Tailings 2 (CT2)	* Tailings Average	Units
Bi	1.3	0.7	1	ppm
Co	22.9	12.7	17.8	ppm
Fe	5.01	2.48	3.745	%
Ga	17.9	20	18.95	ppm
Ge	<0.1	<0.1	<0.1	ppm
Se	2.3	2.5	2.4	ppm

^a Tailings 1 is a batch sample of June 2021 from the rougher flotation tailings of a CP mine. ^b Tailings 2 is a batch sample of March 2023 from the rougher flotation tailings of a CP mine. * Values represent the average assays of the two tailings batches received.

4.1.2. TIMA Studies

TESCAN's integrated mineral analysis (TIMA) was performed using the as-received Tailings 1 (CT1). The results indicate that CT1 has a particle size distribution analysis (PSD) of P_{80} of 135 μm and a median size of 42 μm . However, TIMA was mainly used to identify the major mineral phases in the samples. TIMA's modal chemical group content analysis showed that 91.1% of the minerals in CT are silicates, out of which 16.8% are phyllosilicates. The samples contained 3.91% sulfides, where 0.09% are Cu-sulfides, 2.25% are carbonates, 1.83% are oxides and hydroxides, and 0.83% are phosphates.

Furthermore, the modal distribution of the major minerals in CT consisted mostly of gangue minerals, with 36.5% quartz, 23.6% K-Feldspar, 14.2% biotite, 5.13% albite, 2.23% calcite, 2.17% plagioclase, 2.0% Ca-Mg pyroxenes, 2.03% anorthoclase, 1.86% andradite, 1.55% muscovite, and 1.53% hematite/magnetite. Pyrite was the primary sulfide, accounting for 3.82% of the sample, followed by chalcopyrite at 0.08% in CT.

The initial scan of the CT1 samples did not detect any trace abundance of Te, Au, and Ag minerals. Therefore, a gravity concentration step was carried out using a Mozley Laboratory Mineral Separator with particles less than 100 μm . This was performed to concentrate Te-Au-Ag phases in CT1 for characterization purposes. The concentrates obtained from the gravity separation were analyzed using TIMA bright-phase analysis. The minerals of interest were identified as native gold, electrum, petzite, hessite/argentite, goldfieldite, and tetradymite. The major mineralogical composition of the CT1 Mozley concentrates was found to be 84.75% pyrite, 2.06% hematite/magnetite, and 1.67% galena. Table 3 shows the mineral distribution of Mozley concentrates of CT1 using TIMA bright-phase analysis. It does not include gangue minerals like silicates, phosphates, and carbonates.

Based on the TIMA bright-phase analysis, the distribution of Te among mineral phases in CT1 was as follows: 75% in tetradymite, 15% in petzite, 9.2% in hessite, and 0.5% in other minerals, such as goldfieldite. Additionally, the analysis showed that native gold had the highest Au abundance at 69.8%, followed by petzite with 30.2% Au abundance. Further analysis of CT1 using TIMA revealed that both Te minerals (represented by tetradymite) and Au-Ag minerals were very fine-grained, with all grains being less than 20 μm . The PSD values of tetradymite and Au-Ag minerals were found to be P_{80} at 14 μm and 16 μm , respectively. The liberation analysis of CT1 using TIMA indicated that tetradymite and Au-Ag minerals were mainly present as inclusions in pyrite, and their size was less than 20 μm . According to the data presented in Table 4, at least 93% of tetradymite and Au-Ag minerals are hosted in pyrite, while a minimum of 3% is found as free surface minerals.

Table 3. Mineral composition of Mozley concentrates of CT1 as determined by TIMA.

Mineral	Formula	Mozley Conc. CT (wt.%)
Pyrite	FeS ₂	84.75
Galena	PbS	1.67
Chalcopyrite	CuFeS ₂	0.14
Hematite/Magnetite	Fe ₂ O ₃ /Fe ₃ O ₄	2.055
Tennantite	(Cu,Fe,Zn) ₁₂ As ₄ S ₁₃	0.27
Tetradymite	Bi ₂ Te ₂ S	0.065
Hodrushite	Cu ₄ Bi ₆ S ₁₁	0.01
Petzite	Ag ₃ AuTe ₂	0.03
Hessite	Ag ₂ Te	0.02
Goldfieldite	Cu ₁₂ (Sb,Te) ₄ S ₁₃	0.01
Gold	Au	0.009
CuNi Sulfides	Cu _x Ni _y S _z	0.01
Tetrahedrite	(Cu,Fe,Zn) ₁₂ (Sb,As) ₄ S ₁₃	0.009
Electrum	Au _{0.8} Ag _{0.2}	ND.
Laitakarite	Bi ₄ (Se,S) ₃	ND.

ND = Not detected.

Table 4. Liberation analysis of Te, Ag, and Au minerals in CT1.

Mineral	Tetradymite Locking (wt.%)	Au-Ag Mineral Locking (wt.%)
Pyrite	94.7	93.3
Apatite	0.1	0
Hematite/Magnetite	1.5	0.9
Calcite	0.2	0
Free Surface	3.3	5.7

Findings from characterization studies indicate that Te minerals in CT1 can be enriched if efficient flotation procedures are applied to enrich their hosted sulfide minerals (e.g., pyrite) [28]. Therefore, this study used froth flotation with selected combinations of collectors and frothers to enrich Te minerals.

4.2. Flotation Experiments of Copper Tailings

4.2.1. Effects of Collector Type

The flotation behavior of Te minerals and their host minerals was examined using two types of collectors: EXP300422 (thiocarbamates-based collector) and SIPX, both at a 90 g/t dosage using a 50 g/t MIBC frother. CT1 was used as the flotation feed. Table 5 shows the recovery, grade, and enrichment ratios (ERs). As shown, the results indicate that, when using EXP300422, the recoveries of Te, Au, Ag, and Fe are 51.29%, 48.28%, 61.39%, and 62.82%, respectively. The corresponding enrichment ratios are 0.86, 0.81, 1.03, and 1.05 for Te, Au, Ag, and Fe, respectively.

Similarly, the average recoveries achieved when floating CT1 using SIPX were 61.12%, 44.45%, 62.71%, and 67.46% for Te, Au, Ag, and Fe, respectively. The calculated enrichment ratios were 1.0, 0.73, 1.03, and 1.10 for Te, Au, Ag, and Fe, respectively.

As indicated, the highest overall recovery, grade, and enrichment ratio of Te, the critical mineral of interest, were 61.12%, 0.7 ppm, and 1, respectively, when using SIPX at 90 g/t. The increase in Te recovery was approximately 10% when using SIPX over EXP300422. Results for other elements show a similar trend in grade and recovery. The

results establish a clear overall improvement in flotation performance when using SIPX over EXP30042. Thus, this study also tested the flotation performance of Te, Au, Ag, and Fe when changing the frother type using the optimum collector, SIPX, as established in this set of experiments.

Table 5. Recovery, grade, and enrichment ratios (ERs) of Te, Au, Ag, and Fe with different collectors and 50 g/t MIBC (flotation feed: CT1).

Element	EXP300422 (90 g/t)			SPIX (90 g/t)		
	Recovery	Grade	ER	Recovery	Grade	ER
Tellurium (Te)	51.29%	0.60 ppm	0.86	61.12%	0.70 ppm	1.0
Gold (Au)	48.28%	71 ppb	0.81	44.45%	64 ppb	0.73
Silver (Ag)	61.39%	0.79 ppm	1.03	62.71%	0.79 ppm	1.03
Iron (Fe)	62.82%	5.26 wt. %	1.05	67.46%	5.53 wt. %	1.10

4.2.2. Effects of Frother Type

The aim of this set of experiments was to find the optimum combination of collector/frother systems to enhance the flotation efficiency of Te minerals. As indicated in the previous section, SIPX showed a better performance than EXP300422. Thus, the flotation behavior of Te minerals was further examined as a function of frother type. Two different frothers, MIBC and OREPREP X-237, were used at 50 g/t with 90 g/t SIPX, and CT1 was used as the flotation feed. The results are shown in Table 6.

Table 6. Recovery, grade, and enrichment ratios (ERs) of Te, Au, Ag, Fe, Cu, and S with different frothers (flotation feed: CT1).

Element	SPIX (90 g/t) + MIBC (50 g/t)			SPIX (90 g/t) + OREPREP X-237 (50 g/t)		
	Recovery	Grade	ER	Recovery	Grade	ER
Tellurium (Te)	61.12%	0.70 ppm	1.0	85.30%	1.30 ppm	1.86
Gold (Au)	44.45%	64 ppb	0.73	61.06%	117 ppb	1.33
Silver (Ag)	62.71%	0.79 ppm	1.03	83.51%	1.4 ppm	1.82
Iron (Fe)	67.46%	5.53 wt. %	1.10	64.26%	7.01 wt. %	1.40

As indicated, the experiments performed with OREPREP X-237 show average recoveries of Te, Au, Ag, and Fe of 85.30%, 61.06%, 83.51%, and 64.26%, respectively. Under the same experimental conditions, the corresponding enrichment ratios were 1.86, 1.33, 1.82, 1.40, 1.40, and 2.13.

The results from this set of experiments show that the highest overall recovery of Te is 85.30% when using OREPREP X-237 at 50 g/t, which is a 24.18% increase in Te recovery compared to MIBC. The highest grade and enrichment values for the same experimental conditions were 1.30 ppm and 1.86, respectively. The results for other elements show a comparable increase in grade and recovery when using OREPREP, except for Fe. Iron recovery decreased by only 3.2% with OREPREP X-237 compared to MIBC.

The results from Sections 4.2.1 and 4.2.2 establish a clear improvement in the flotation performance of Te when using SIPX over EXP300422 and OREPREP X-237 over MIBC at 90 g/t and 50/g dosages, respectively. However, although the recovery obtained for Te was positive, the maximum enrichment ratio obtained for Te was 1.86. The low enrichment and high recovery results present a new problem. The hypothesized problem was attributed to the high presence of slimes within CT, where more than 80% of <38 µm size fractions were mainly silicates and micas (phyllosilicates) that could potentially increase the overall mass recovery while lowering the enrichment of Te, Au, Ag, and Fe. Therefore, this study proposed using additional physical separation steps for the preconcentration of CT

by removing these fine materials (desliming). The authors proposed using the gravity separation process to preconcentrate the CT prior to froth flotation, as discussed in the following sections.

4.3. Gravity Separation of Copper Tailings

As stated in Section 3.2.2, the GS experiments were performed using Tailings 2 (CT2) as the feed, different solid-to-liquid (S:L) ratios, and standard parameters. The results for GS experiments 1, 2, and 3 with S:L ratios of 1:15, 1:10, and 1:5, respectively, are shown in Tables 7–9. The findings from the GS experiments indicate that the highest combined recoveries of Te, Au, and Ag are achieved at an S:L of 1:15. At this ratio, the combined recoveries for Te, Au, and Ag in the concentrate and middling streams were 69.53%, 74.37%, and 68.26%, respectively. The highest combined recovery for Fe was approximately 70%, shared by the S:L ratios 1:10 and 1:15. These results informed the decision to use the GS concentrate and middling (GS-C+M) combined streams as the flotation feed.

Table 7. Recovery and enrichment values of Te, Au, Ag, and Fe using the gravity separation process (Wilfley shaking table) where S:L = 1:15 (flotation feed: CT2).

Element	Concentrate			Middlings			Tailings		
	Recovery	Grade	ER	Recovery	Grade	ER	Recovery	Grade	ER
Tellurium (Te)	42.98%	0.63 ppm	1.58	26.55%	0.28 ppm	0.70	28.36%	0.30 ppm	0.75
Gold (Au)	44.08%	168 ppb	1.62	30.29%	105 ppb	1.01	24.28%	93 ppb	0.89
Silver (Ag)	29.73%	0.99 ppm	1.46	38.53%	0.87 ppm	1.28	28.33%	0.96 ppm	1.41
Iron (Fe)	32.85%	3.44 wt. %	1.39	34.05%	2.88 wt. %	1.16	32.30%	2.95 wt. %	1.19

Table 8. Recovery and enrichment values of Te, Au, Ag, and Fe using the gravity separation process (Wilfley shaking table) where S:L = 1:10 (flotation feed: CT2).

Element	Concentrate			Middlings			Tailings		
	Recovery	Grade	ER	Recovery	Grade	ER	Recovery	Grade	ER
Tellurium (Te)	32.89%	0.30 ppm	0.75	3.71%	0.20 ppm	0.50	44.76%	0.30 ppm	0.75
Gold (Au)	50.18%	119 ppb	1.14	6.85%	96 ppb	0.92	29.41%	66 ppb	0.63
Silver (Ag)	44.50%	0.69 ppm	1.01	5.57%	0.51 ppm	0.75	45.93%	0.85 ppm	1.25
Iron (Fe)	34.79%	2.68 wt. %	1.08	33.83%	2.45 wt. %	0.99	28.84%	2.82 wt. %	1.14

Table 9. Recovery and enrichment values of Te, Au, Ag, and Fe using the gravity separation process (Wilfley shaking table) where S:L = 1:5 (flotation feed: CT2).

Element	Concentrate			Middlings			Tailings		
	Recovery	Grade	ER	Recovery	Grade	ER	Recovery	Grade	ER
Tellurium (Te)	18.51%	0.50 ppm	1.25	15.39%	0.20 ppm	0.50	59.75%	0.30 ppm	0.75
Gold (Au)	17.41%	159 ppb	1.53	15.61%	83 ppb	0.80	60.57%	84 ppb	0.81
Silver (Ag)	13.81%	1.38 ppm	2.03	6.34%	0.40 ppm	0.59	64.38%	0.66 ppm	0.97
Iron (Fe)	10.87%	3.96 wt. %	1.60	9.13%	2.10 wt. %	0.85	78.74%	2.57 wt. %	1.04

4.4. Froth Flotation of Gravity Separation Products

Based on the gravity separation results, the researchers opted to use the combined middling and concentrate products from the GS experiments, also referred to as GS-C+M, as the flotation feed in this set of experiments, as these were deslimed CT2. GS-C+M was floated according to the optimum dosages tested for the xanthate (SIPX) collector and

glycol (OREPREP X-237) frother. The results of the flotation experiments of GS-C+M are shown in Figure 3.

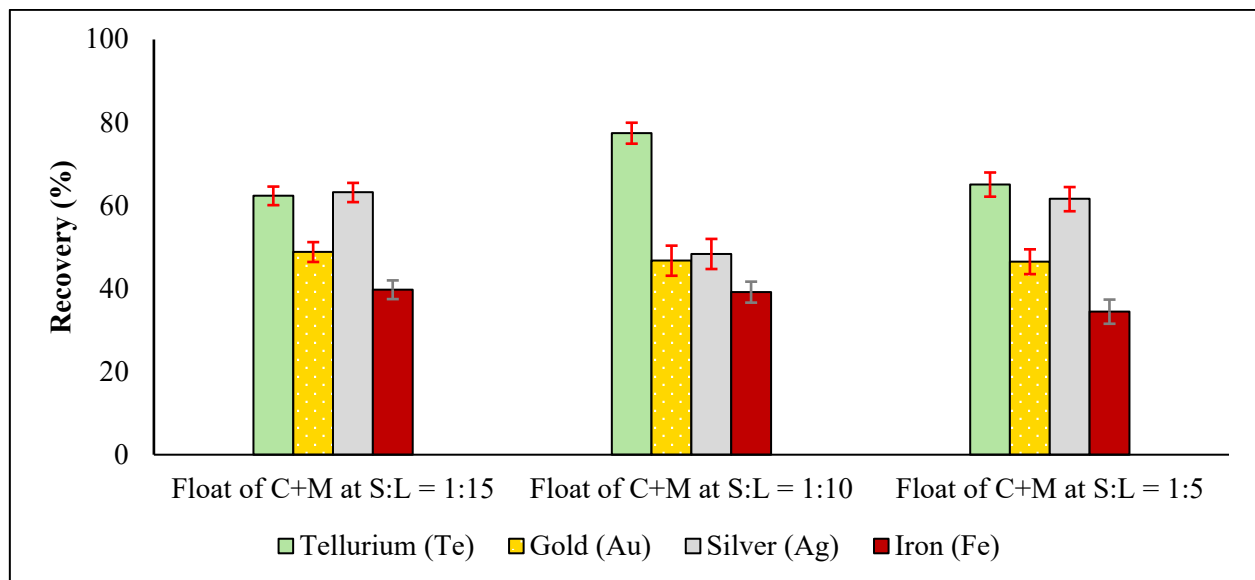


Figure 3. Recoveries of Te, Au, Ag, and Fe when using GS middling and concentrate (C+M), produced at varying S:L ratios as the flotation feed.

As indicated, the average recovery achieved for the flotation of GS-C+M at an S:L of 1:15 was 63.33%, 48.80%, 63.22%, and 39.72% for Te, Au, Ag, and Fe, respectively. The corresponding enrichment ratios were calculated as 0.88, 1.45, 2.45, and 2.08. Table 10 summarizes the recoveries, grades, and enrichment ratios of Te, Au, Ag, and Fe after the flotation of C+M-GS at an S:L of 1:15.

Table 10. Recoveries, grades, and enrichment ratios (ERs) of Te, Au, Ag, and Fe after the flotation of concentrates and middlings produced from gravity separation where S:L = 1:15.

Element	Recovery	Grade	ER
Tellurium (Te)	62.33%	0.70 ppm	0.88
Gold (Au)	48.80%	289 ppb	1.45
Silver (Ag)	63.22%	1.89 ppm	2.45
Iron (Fe)	39.72%	5.24 wt.%	2.08

The average recoveries achieved when floating the C+M obtained from the gravity separation process at a 1:10 S:L were 77.43%, 46.72%, 48.32%, and 39.13% for Te, Au, Ag, and Fe, respectively. Furthermore, the enrichment ratios were 13, 6.53, 4.57, and 5.67 for Te, Au, Ag, and Fe, respectively. Table 11 shows the recoveries, grades, and enrichment ratios of Te, Au, Ag, and Fe after the flotation of C+M-GS obtained at an S:L ratio of 1:10.

Table 11. Recoveries, grades, and enrichment ratios (ERs) of Te, Au, Ag, and Fe after the flotation of concentrates and middlings produced from gravity separation where S:L = 1:10.

Element	Recovery	Grade	ER
Tellurium (Te)	77.43%	3.90 ppm	13.00
Gold (Au)	46.72%	699 ppb	6.53
Silver (Ag)	48.32%	3.11 ppm	4.57
Iron (Fe)	39.13%	14.00 wt.%	5.67

Similarly, floating C+M produced from the gravity separation process where S:L = 1:5 resulted in 65.05%, 46.47%, 61.62%, and 34.45% recovery rates for Te, Au, Ag, and Fe, respectively. The corresponding enrichment ratios were 9.5, 6.61, 7.36, and 4.26. Table 12 shows the recoveries, grades, and enrichment ratios of Te, Au, Ag, and Fe after the flotation of C+M-GS obtained at an S:L ratio of 1:5.

Table 12. Recovery and grade values of Te, Au, Ag, and Fe after the flotation of concentrates and middlings produced from gravity separation where S: L = 1:5.

Element	Recovery	Grade	ER
Tellurium (Te)	65.05%	1.90 ppm	9.50
Gold (Au)	46.47%	753 ppb	6.61
Silver (Ag)	61.62%	5.08 ppm	7.36
Iron (Fe)	34.45%	10.30 wt. %	4.26

The results indicate that the processing of the GS-C+M at an S:L of 1:10 using froth flotation achieved the highest recovery, grade, and enrichment for Te. Although the other S:L ratios tested performed better for Au, Ag, and Fe, this study mainly focuses on understanding the possibility of enriching Te minerals and characterizing the existing streams to highlight a path forward for process optimization. Nevertheless, ICP-MS results alone could not provide a clear indication of the geometallurgical link between Te-Au-Ag and Fe-Cu-S and the mineral phases represented in the GS and froth flotation process products. Therefore, to gain deeper insights, the researchers conducted TIMA on the streams that showed the highest recovery and grade for Te (shown in Figure 4 in red arrows).

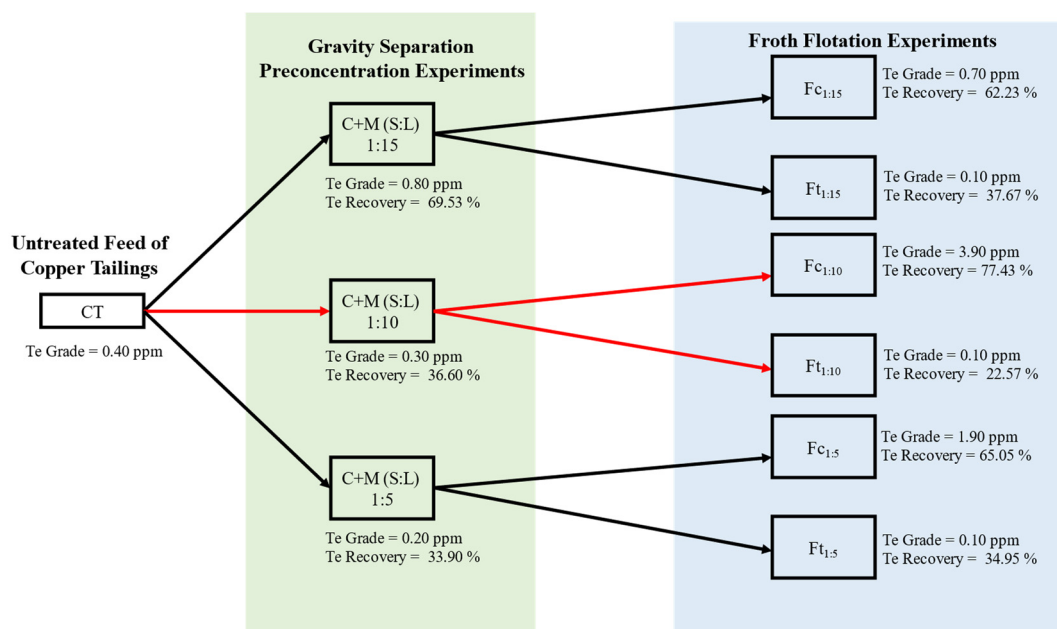


Figure 4. Flowsheet diagram of gravity separation (light green) and froth flotation (light blue) experiments. The red arrows highlight the streams with the highest final Te concentration. Copper tailings or as-received tailings (Tailings 2 was used for all the experiments) are shown as CT. The gravity separation concentrates and middling combination or flotation feed are presented as (C+M), and the solid-to-liquid ratio is shown as S:L. Lastly, flotation concentrates and tailings are indicated by Fc1:# and Ft1:# with the 1:# subscript referring to the S:L from gravity separation experiments.

4.5. TIMA Analysis of Physical Separation Products

In this section, the streams analyzed for TIMA included the combined concentrate and middling (C+M) products of gravity separation (GS) produced at an S:L of 1:10, which is referred to as the flotation feed, and the concentrate and tailing products of the flotation experiments conducted using this feed. These streams were selected based on achieving the highest recovery for Te in the final concentrate product, as shown in Figure 4.

4.5.1. Particle Size Distribution (PSD)

Figure 5 shows the PSD for the flotation feed, concentrates, and tailings. P_{80} was 156 μm for the flotation feed, 161 μm for the flotation tailings, and 49 μm for the flotation concentrate. The corresponding median particle sizes were 65 μm , 80 μm , and 21 μm .

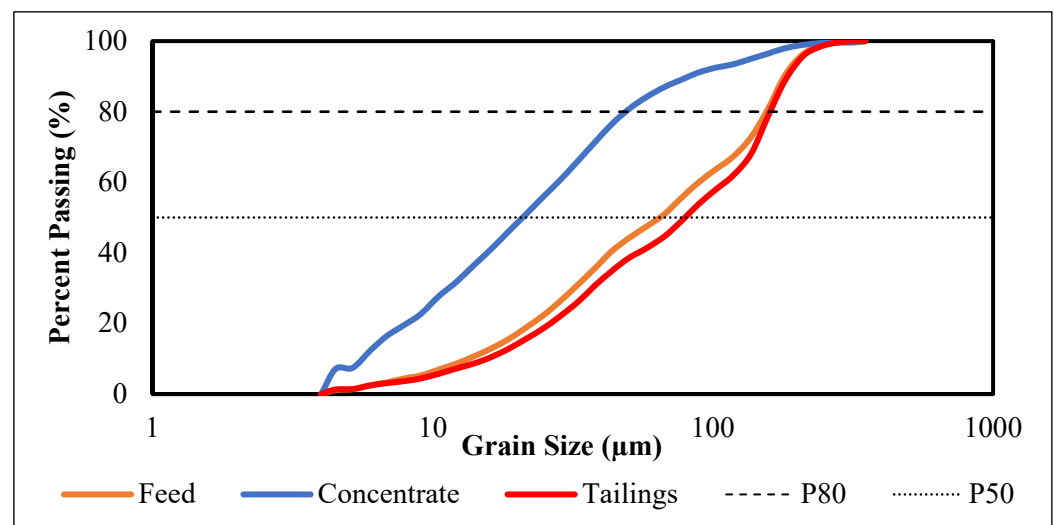


Figure 5. Particle size distribution (PSD) for the flotation feed (orange), concentrate (blue), and tailings (red). P_{80} is shown as a dashed line, and the mean is shown as a round dotted line. [Flotation Feed = concentrate and middling (C+M) products of gravity separation (GS) produced at an S:L of 1:10].

Chalcopyrite's grain size was the largest in the flotation feed, with a median size of 104 μm and a P_{80} of 184 μm . In contrast, the flotation tailings exhibited the smallest chalcopyrite grain sizes, with a median of 35 μm and a P_{80} of 63 μm . The flotation concentrates had intermediate chalcopyrite grain sizes, with a median of 79 μm and a P_{80} of 156 μm . In the feed, concentrates, and tailing flotation streams, pyrite grain size distribution varied notably across different concentration steps. In the feed, pyrite grains were relatively coarse, with a median size of 64 μm and a P_{80} of 142 μm . The concentrates had the largest pyrite grain sizes, with a median of 94 μm and a P_{80} of 149 μm . In contrast, tailings showed the smallest grain sizes, with a median of 34 μm and a P_{80} of 114 μm . Figure 6 shows the grain size distribution for pyrite in the flotation feed, concentrates, and tailings. This suggested that larger pyrite grains tend to be less successfully recovered in the flotation process, possibly due to incomplete liberation or mechanical entrainment in the waste stream, explored in detail in Section 4.5.5 and in the discussion.

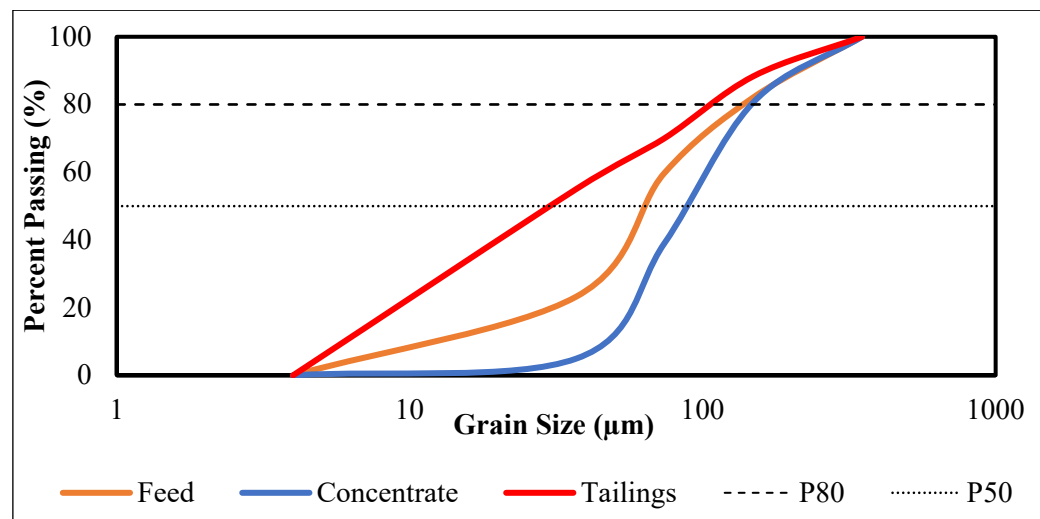


Figure 6. Pyrite's grain size distribution for the flotation feed (orange), concentrate (blue), and tailings (red). P80 is shown as a dashed line, and the mean is shown as a round dotted line. [Flotation Feed = concentrate and middling (C+M) products of gravity separation (GS) produced at an S:L of 1:10].

4.5.2. Mineral Content and Phase Identification

TIMA was used to determine the total mineral content by chemical groupings, as shown in Table 13. The total sulfides were 23.8% in the flotation concentrate, 2.18% in the flotation feed or C+M S:L = 1:10, and 0.17% in the flotation tailings, due mainly to pyrite. The copper sulfides comprised 1.07% of the sulfides in the flotation concentrate, 0.34% in the flotation feed, and 0.04% in the flotation tailings, due mainly to chalcopyrite. Total silicates were 94% in the flotation, 72.7% in the flotation concentrate, and 96% in the flotation tailings. Additionally, phyllosilicates (i.e., clays and micas) content was 13% in the flotation feed, 12.4 in the flotation tailings, and 15% in the flotation concentrates.

Table 13. Mineral content of flotation feed, flotation concentrate, and flotation tailings presented by chemical grouping.

Chemical Group	Flotation Feed (wt.%)	Flotation Concentrate (wt.%)	Flotation Tailing (wt.%)
Total Silicates	94	72.7	96
Silicates	81	57.7	83.6
Phyllosilicates	13	15	12.4
Total Sulfides	2.18	23.8	0.17
Carbonates	1.88	1.43	1.92
Phosphates	0.9	0.77	1.01
Oxide/Hydroxides	0.5	0.51	0.56

[Flotation Feed = concentrate and middling (C+M) products of gravity separation (GS) produced at an S:L of 1:10].

Table 14 shows the modal mineral concentrations for flotation feed, flotation concentrate, and flotation tailings. Chalcopyrite was the most abundant copper-bearing mineral in all the streams observed, and this was expected as the flotation feed was composed of CT. Chalcopyrite content in the flotation concentrates was 1.50%, with 0.33% in the flotation feed and 0.04% remaining in the flotation tailings. Bornite was a trace copper mineral that was found at 0.04% in the flotation concentrate and not detected in the flotation feed or tailings. Other metal sulfides were molybdenite and sphalerite, which were found at 0.16% and 0.04% in the flotation concentrates, respectively. Pyrite was the primary sulfide and

was 24.6% in the flotation concentrates, as compared to 1.82% in the flotation feed and 0.04% in the flotation tailings.

Table 14. Mineral content for flotation feed, flotation concentrate, and flotation tailings classified by mineral phase.

Mineral	Formula	Flotation Feed (wt.%)	Flotation Concentrate (wt.%)	Flotation Tailing (wt.%)
K-Feldspar	KAlSi_3O_8	36.10	27.40	36.50
Quartz	SiO_2	37.30	22.90	39.50
Biotite	$\text{K}(\text{Mg},\text{Fe})_3(\text{Al},\text{Fe})\text{Si}_3\text{O}_{10}(\text{OH})_2$	9.90	10.90	9.33
Pyrite	FeS_2	1.82	24.60	0.13
Plagioclase	$\text{Na}_{0.5-0.3}\text{Ca}_{0.5-0.7}\text{Al}_{1.5-1.7}\text{Si}_{2.5-2.3}\text{O}_8$	5.04	3.43	5.05
Muscovite	$\text{KAl}_2(\text{Si}_3\text{Al})\text{O}_{10}(\text{OH})_2$	1.36	1.07	1.41
Phlogopite	$\text{KMg}_3\text{Si}_3\text{AlO}_{10}(\text{OH})_2$	1.17	1.4	1.13
Chalcopyrite	CuFeS_2	0.33	1.5	0.04
Garnet	$(\text{Fe},\text{Ca},\text{Mg})_3(\text{Fe},\text{Al})(\text{SiO}_4)_3$	0.52	0.13	0.66
Chlorite	$(\text{Fe},\text{Mg})_5\text{Al}(\text{Si}_3\text{Al})\text{O}_{10}(\text{OH})_8$	0.37	0.45	0.32
Pyroxene	$(\text{Ca},\text{Na})(\text{Mg},\text{Fe},\text{Al},\text{Ti})(\text{Si},\text{Al})_2\text{O}_6$	0.35	0.21	0.42
Kaolinite	$\text{Al}_2\text{Si}_2\text{O}_5(\text{OH})_2$	0.16	0.25	0.16
Amphibole	$\text{Ca}_2(\text{Mg},\text{Fe},\text{Al})_5(\text{Al},\text{Si})_8\text{O}_{22}(\text{OH})_2$	0.12	0.14	0.14
Talc	$\text{Mg}_3\text{Si}_4\text{O}_{10}(\text{OH})_2$	0.04	0.12	0.04
Molybdenite	MoS_2	0.01	0.16	ND
Zircon	ZrSiO_4	0.03	0.02	0.03
Titanite	CaTiSiO_5	0.02	0.02	0.02
Bornite	Cu_5FeS_4	ND	0.04	ND

[Flotation Feed = concentrate and middling (C+M) products of gravity separation (GS) produced at an S:L of 1:10].

Primary non-sulfide gangue minerals were K-Feldspar and quartz at 36%–37% and 37%–40%, respectively, in the flotation feed and tailings, while K-Feldspar was reduced to 27% and quartz to 23% in the flotation concentrates. Biotite was a gangue mineral that ranged between 9% and 10% in the flotation feed and tailings, respectively, and was 11% in the concentrates. Plagioclase was approximately 5% in both the flotation feed and tailings and 3.4% in the flotation concentrates. Calcite was 1.8% to 1.9% in the flotation feed and tailings, respectively, and 1.3% in the flotation concentrates. Tellurium, gold, and silver minerals were less than 0.01% in the modal mineral content and were not reported.

Furthermore, TIMA mineral content was used to calculate the recovery and deportment of the major minerals in the flotation feed, concentrates, and tailings, as shown in Section 4.5.5.

4.5.3. Major Sulfide Locking/Liberation

In all the samples, chalcopyrite was locked primarily in the major gangue minerals, K-Feldspar, and quartz. The free surface values were high in the flotation feed (75%) and concentrate (71.1%) samples and lowest in the tailings (24.8%), which correlates to the PSD.

Moreover, pyrite was locked primarily in K-Feldspar and quartz, as well (Table 15). Pyrite was well-liberated in both the flotation feed and concentrate, with decreased liberation in the tailings, which is reflected by the free surface. This suggests that liberated or free surface pyrite grains were not successfully recovered in the flotation process, possibly due

to mechanical entrainment in the waste stream and not because of incomplete liberation from gangue minerals.

Table 15. Pyrite locking and liberation analysis of flotation feed, concentrates, and tailings.

Mineral	Flotation Feed	Flotation Tailings	Flotation Concentrates
K-Feldspar	2.9	9.9	1.6
Quartz	3	5.8	2.3
Biotite	1	2.6	0.7
Plagioclase	0.5	1	0.3
Calcite	0.1	1	0.1
Ca Mg Aluminosilicate	0.1	0.8	0.1
Chalcopyrite	0.3	0.3	0.3
Muscovite	0.2	0.2	0.1
Phlogopite	0.1	0.1	0.1
Free Surface	90.8	77.4	93.9

[Flotation Feed = concentrate and middling (C+M) products of gravity separation (GS) produced at an S:L of 1:10].

The results show that mineral associations are complex, but consistently show that chalcopyrite and pyrite are primarily locked with K-Feldspar and quartz across all samples from the flotation streams. The analysis highlighted the need for TIMA bright-phase analysis, which focuses on particles containing minerals with high MAN, like gold and tellurium, to reveal crucial information about the distribution of these elements of interest within our flotation streams.

4.5.4. Tellurium Mineralogy and Locking/Liberation

Tellurium mineralogy in the flotation feed and concentrates was predominantly characterized by the Te minerals tetradymite, altaite, and petzite; no Te minerals were found in the flotation tailings. Tellurium minerals were found nearly exclusively in the flotation concentrate, as seen in Figure 7. The 11 grains of tetradymite identified were all less than 12 µm in the flotation concentrate, and the only grain found in the flotation feed sample was less than 5 µm. Singular grains of petzite and altaite were 7 µm and 92 µm, respectively, and both were identified in the flotation concentrates. Therefore, the most substantial presence of Te was observed in the flotation concentrates, where altaite accounted for approximately 88.7% of tellurium distribution, making it the primary carrier of tellurium. Tetradymite, though presented across multiple samples, was more significantly found in the concentrates, contributing to 10.8% of the Te content; however, they were much finer than the relatively large altaite grains. Petzite was detected to a lesser extent, representing only 0.4% of the total Te content in concentrates.

Table 16 shows a summary of the results for Te mineral locking and liberation analysis based on the mass (%) of all Te-bearing minerals. Locking characteristics revealed that Te minerals were mainly locked with quartz in the flotation concentrates, constituting 23.6% of the mineral locking mass. Interestingly, in the flotation feed samples, all tetradymite particles were associated with pyrite, highlighting a significant interaction between these two minerals, as shown in Table 17. In the concentrate samples, Te was also found in a free form to a significant degree, suggesting relatively good liberation at 63.6% of Te minerals not being locked with gangue minerals.

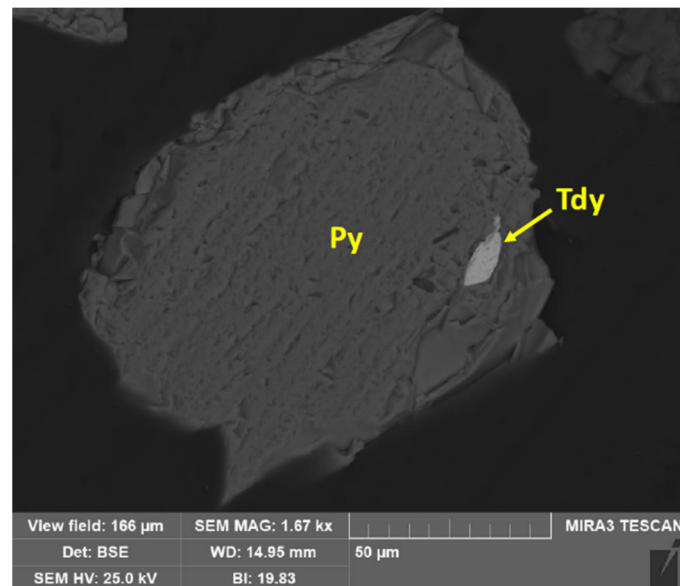


Figure 7. SEM-BSE image showing a tetradymite (Tdy) grain of 15 µm locked in a pyrite (Py) grain found in the flotation concentrates.

Table 16. Locking and liberation analysis based on mass (%) of all Te minerals (altite, petzite, and tetradymite).

Mineral	Flotation Feed	Flotation Tailings	Flotation Concentrates
Pyrite	100	0	9.8
Quartz	0	0	23.6
K-Feldspar	0	0	2.3
Muscovite	0	0	0.8
Free Surface	0	0	63.6

[Flotation Feed = concentrate and middling (C+M) products of gravity separation (GS) produced at an S:L of 1:10].

Table 17. Locking and liberation analysis based on mass (%) of tetradymite.

Mineral	Flotation Feed	Flotation Tailings	Flotation Concentrates
Pyrite	100	0	82.1
Quartz	0	0	0
K-Feldspar	0	0	0
Muscovite	0	0	0
Free Surface	0	0	17.8

[Flotation Feed = concentrate and middling (C+M) products of gravity separation (GS) produced at an S:L of 1:10].

4.5.5. Mineral Recovery and Deportment Calculations

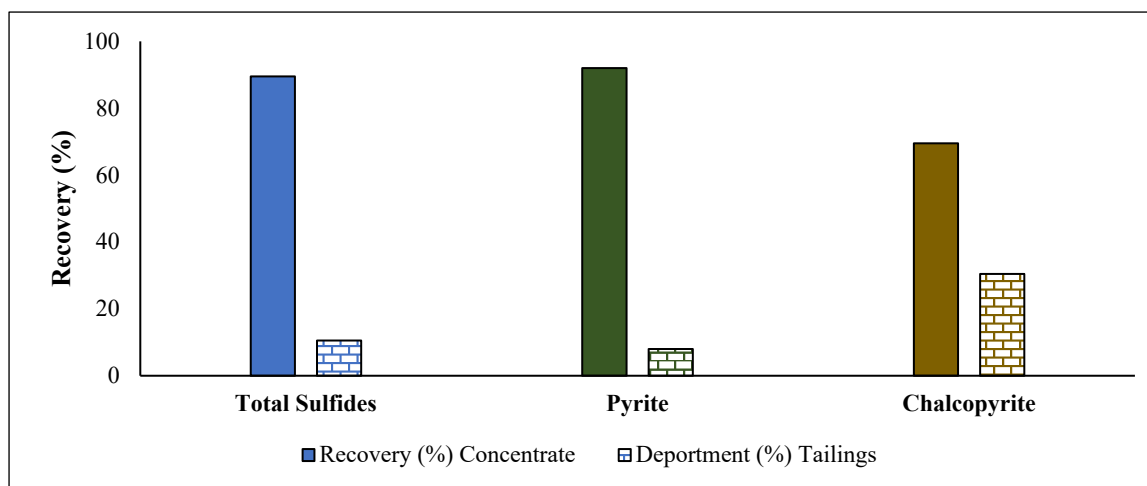
TIMA revealed important results regarding the behavior of Te mineral hosts (such as pyrite) and the associated minerals, such as phyllosilicates, which could have a negative impact on the flotation performance of the gravity separation C+M at a solid-to-liquid ratio of 1:10. Total sulfide and total silicate recovery were measured as 89.5% and 4.41%, respectively, for the flotation concentrate. Deportment to the tailings was 10.50% and 95.59% for total sulfide and total silicate, respectively. Table 18 shows the recovery and grade for the major mineral chemical groups of flotation concentrates and tailings.

Table 18. Recovery and grade of major minerals in flotation concentrates and tailings.

Chemical Group	Concentrate Grade (wt.%)	Recovery (%) Concentrate	Tailing Grade (wt.%)	Department (%) Tailings
Total Silicates	72.7	4.41	96	95.59
Silicates	57.7	4.03	83.60	95.97
Phyllosilicates	15	6.86	12.40	93.14
Total Sulfides	23.8	89.50	0.17	10.50
Carbonates	1.43	4.34	1.92	95.66
Phosphates	0.77	4.43	1.01	95.57
Oxide/Hydroxides	0.51	5.25	0.56	94.75

[Flotation Feed = concentrate and middling (C+M) products of gravity separation (GS) produced at an S:L of 1:10].

Figure 8 presents a detailed composition of the total sulfide department and recovery from gravity separation C+M at an S:L of 1:10. Pyrite, the major sulfide determined by TIMA and our main host for Te minerals, accounted for 92.01% of recovery and 7.99% of department. It is important to mention that 55% of the pyrite deported to the tailings was within the less than 38 μm size fraction, while 95% of the pyrite recovered was in the greater than 38 μm size fraction. Additionally, chalcopyrite recovery and department were 69.54% and 30.46%, respectively. Similar behavior was observed for size fractions' recovery, where 98% of chalcopyrite was recovered in the greater than 38 μm size fraction. However, department was slightly different, with only 16% within the less than 38 μm size fraction.

**Figure 8.** Recovery and department of sulfide minerals in flotation products. [Flotation Feed = concentrate and middling (C+M) products of gravity separation (GS) produced at an S:L of 1:10].

As for the silicate content, the researchers focused on understanding the flotation of phyllosilicates to characterize their impact after the desliming step of CT. Total phyllosilicate recovery and department were 6.86% and 93.14%, respectively, while micas', like biotite, muscovite, phlogopite, and chlorite, recovery rates were in the range of 4–8%, with more than 90% of micas deporting to the tailings, as observed in Figure 9. Looking at the clay minerals present in the sample, kaolinite had a similar flotation behavior to micas, with 8.68% and 91.32% results for recovery and department, respectively. However, talc flotation behavior was completely different from that of the other clay minerals. Talc recovery was 15.44% and department to the tailings was 84.56%. The detailed results of the total phyllosilicate department and recovery are shown in Figure 9.

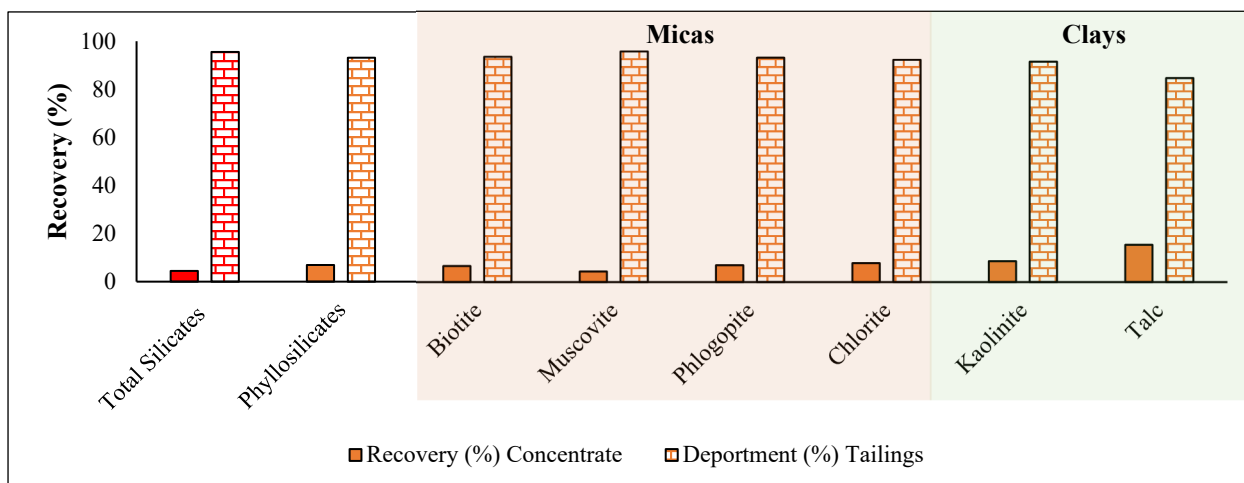


Figure 9. Recovery and deportment of total silicates in flotation products. [Flotation Feed = concentrate and middling (C+M) products of gravity separation (GS) produced at an S:L of 1:10].

5. Discussion

5.1. Characterization of Copper Tailing

Characterization studies of copper tailings provided key insights that directly impacted the design of the mineral processing experiments. The mineralogical analysis by TIMA revealed that the CT samples had PSD with a P_{80} of 135 μm and a median size of 42 μm , indicating a substantial presence of fine particles. Approximately 80% of fine particles (less than 38 μm) identified were silicates, specifically 36.2% quartz, 20.3% K-Feldspar, 18% biotite, and 4.85% albite. Several studies suggested that silicate fine particles could negatively impact different concentration procedures during beneficiation, especially froth flotation, where fine particles produce slime coatings, increase slurry viscosity, and increase reagent consumption due to their large surface area [44–51]. The presence of clay minerals, like biotite and muscovite (hydrophilic clays), increases the viscosity of the slurry, impacting the slurry's flowability, which requires more conditioning time and/or a higher dosage [52,53]. Other clay minerals, like talc (hydrophobic clays), impact the froth phase and may provide stability to the froth layer, but will form slimes that reduce the hydrophobicity of valuable minerals [52–54].

The characterization analysis showed that the CT contained an average Te grade of 0.40 ppm, with Te and associated valuable minerals being 93% locked within pyrite grains, which predominantly measured less than 20 μm in size. These findings also underscore the necessity of employing a preconcentration step to deslime the material and enhance the flotation efficiency of Te minerals or Te mineral hosts by reducing fine particle interference.

Unlike previous findings, which focused on selective flotation for Au-tellurides from pyrite in gold ores [55], our approach extends the application of flotation techniques to CT, a novel source for Te and Au recovery. This direct utilization of CT, as opposed to ore or concentrated pyrite, marks a significant contribution to the field of critical mineral recovery. However, this research's main limitation was the reliability of Te concentration across different tailing samples, suggesting a need for the site-specific adaptation of the process.

Furthermore, the detailed mineralogical study highlighted that pyrite was the primary host for Te, Au, and Ag, with other sulfide minerals, like chalcopyrite, being less prevalent. This informed the decision to use froth flotation to further concentrate Te-bearing phases. The successful concentration of the pyrite-hosted telluride approach will require further processing that begins with the regrinding of pyrite to liberate telluride minerals or roasting for oxidation and the fracture of the host mineral to allow for Te leaching. However, the overall economic feasibility of the process heavily depends on the marked association between Te and Au-Ag minerals.

5.2. Mineral Concentration Studies

5.2.1. Impact of Collector Type

As discussed in Section 4.2, the optimum flotation efficiency of the Te mineral was achieved using SIPX (xanthate), which performed better than EXP300422 (thiocarbamate). In fact, the mechanism of the adsorption of xanthate and thiocarbamate collectors on the pyrite surface is different, which could result in different stabilities of the formed species after adsorption, which in turn impacts the bubble–particle attachment and thus the overall flotation performance. The adsorption of xanthates on pyrite surfaces involves both chemical and electrochemical processes, significantly influenced by the electrochemical conditions of the pulp.

The results from Sections 4.3–4.5 show how the floatability of pyrite is influenced by the type of collector used for flotation in alkaline media (pH 8). At this pH range, the adsorption of xanthate involves both chemisorption and electrochemical processes, which result in the formation of stable ferric xanthate compounds and dixanthogen complexes [56–59]. These compounds enhance the hydrophobicity of pyrite and the stability of the bubble–particle aggregates formed, therefore improving the flotation efficiency. In contrast, thiocarbamate complexes formed on the surface of pyrite through chemisorption are known to be stable at slightly acidic to neutral pH conditions, but become less stable in an alkaline pH. These differences in the stability and the nature of hydrophobic species formed by the two collectors resulted in different flotation outcomes, with xanthate outperforming thiocarbamate. However, more fundamental studies should be conducted to understand the adsorption mechanism, which will be the focus of our future work.

5.2.2. Gravity Separation Studies

The gravity separation experiments aimed to preconcentrate Te from CT using the Wilfley Table by creating three distinct streams: concentrate, middlings, and tailings. While gravity separation was effective for desliming and handling high silicate and mica contents, it did not achieve significant separation efficiency for Te due to its fine dissemination within the pyrite matrix. For instance, the highest Te recovery achieved was only 42.98% at a grade of 0.63 ppm for the concentrates when testing the S:L ratio of 1:15. The low recovery results are consistent with the mineralogical characterization, which indicated that over 90% of Te minerals were locked within pyrite grains, predominantly as fine inclusions less than 20 μm . This aligns with the findings from the broader literature that indicate gravity separation is less effective for finely disseminated minerals, which require secondary concentration methods, such as flotation, for effective recovery [60,61].

Despite the widespread adoption of gravity separation due to its low operational cost and simplicity, its effectiveness can vary significantly based on the mineralogical characteristics of the tailings. A previous study [38] reviewed the gravity separation process used to upgrade copper minerals from CT. The researchers observed that, despite the higher efficiency and low installation cost of gravity separation, it is only feasible when there is a significant difference in specific gravity between the valuable minerals and the gangue.

The limited efficacy of gravity separation experiments highlights the need for more efficient desliming techniques, such as the use of specially designed hydrocyclone classifiers for fine particle separation. Exploring fine or ultra-fine grinding after gravity separation might enhance Te mineral liberation, but would also increase processing costs and energy consumption. Alternatively, optimizing froth flotation processes has shown promise in improving recovery rates for such finely disseminated minerals. Several studies have shown that flotation can significantly enhance recovery by selectively targeting minerals for flotation based on surface chemistry, something that gravity separation alone cannot achieve [35,60,62,63].

5.2.3. Froth Flotation Studies of GS Preconcentrates

The best flotation efficiency of Te minerals was achieved when using the preconcentrated CT (or GS-C+M) produced at an S:L = 1:10 as the flotation feed with 90 g/t of xanthate (SIPX) collector and 50 g/t of glycol (OREPREP X-237) frother. At these conditions, the Te recovery, grade, and enrichment ratio were 77.43%, 3.90 ppm, and 13, respectively. By using gravity separation as a preconcentration step, the froth flotation process was refined to effectively recover Te-Au-Ag minerals hosted and liberated from their host minerals in the context of the complex gangue mineralogy of CT. One of the primary reasons for the relatively low recovery of Te in this study can be attributed to the mineral's fine dissemination within the pyrite host and surface oxidation. Several authors have suggested that fine-grained dissemination often leads to inadequate liberation during the grinding process, resulting in lower recovery rates during flotation [64–70]. Moreover, the presence of other sulfide minerals, such as chalcopyrite and pyrite, which are frequently associated with telluride minerals, further complicates the separation process due to their comparable flotation behavior when using conventional reagents schemes [64,71].

Pyrite (Te host mineral) activation is another factor influencing the flotation process. Pyrite is a theoretically highly floatable mineral at a neutral to acidic pH. However, pyrite in copper tailings is usually a “depressed” form of the mineral with adsorbed layers of cyanides or other chemicals used to suppress pyrite's flotation. Therefore, pyrite activation may be considered for enhanced enrichment [72–77]. Pyrite can be activated by the addition of metal ions, such as copper [78]. The addition of copper sulfate as an activator in flotation processes can significantly improve the recovery of pyrite, which should be considered in the context of recovering Te minerals hosted in pyrite [79–82].

Lastly, looking at the selective flotation of Te minerals, there is limited literature on the fundamental studies of the surface adsorption of collectors on Te minerals. Several authors have conducted crucial research on the adsorption of reagents on synthetic telluride surfaces. Merkle et al. (2002) produced synthetic tellurides used in the studies analyzing telluride surfaces and the synthetic materials after Ni-Cu-PGE mineralization in the Merensky Reef, Bushveld Igneous Complex, South Africa [83]. Veermaak (2005) extensively analyzed electrochemical potential, contact angle, and performed microflotation analysis on synthetic PGE tellurides [84]. In other studies, synthetic Pd-Bi-Te electrodes showed a minimal difference in current–potential curves with and without the addition of a potassium ethyl xanthate (PEX) collector. In the same synthetic Pd-Bi-Te system, contact angle measurements of 63° suggest a high hydrophobicity potential [84,85]. The same Pd-Bi-Te electrode system was analyzed using Raman spectroscopy in a 0.05 M sodium tetraborate solution with 1 mM PEX. Xanthate formation was detected in less than 120 s and formed a hydrophobic layer with the synthetic Pd-Bi-Te electrode [84–87]. Finally, microflotation tests conducted at pH 9 using an 80 g/t PEX collector achieved a 97% recovery of Pd-Bi-Te synthetic tellurides, suggesting a high selectivity of PEX toward Pd-Bi-Te compounds [84,88,89]. Shackleton and Shackleton et al. (2007) performed fundamental surface chemistry tests on synthetic Pd-Bi-Te compounds and compared the differences in floatability between sulfides, arsenides, and tellurides. XPS and ToF-SIMS showed that xanthate selectively absorbs on the surfaces of Pd-Bi-Te compounds rather than on base metal sulfides and arsenides [90,91]. The studies presented provide valuable insights into the surface adsorption behavior and mechanisms of synthetic Te materials. However, further efforts should be made to explore telluride surface chemistry and adsorption behavior with different reagent systems and various Te mineral and synthetic material compositions, with an emphasis on Au-Ag-Te compositions. This exploration is necessary to optimize the Te mineral flotation process. In summary, flotation results indicate that the multi-stage concentration approach, optimization of reagent dosage, an understanding of the collector–mineral adsorption mechanism, and possible activation of Te host minerals (e.g., pyrite) prior to collector adsorption could enhance flotation efficiency [90,91].

6. Conclusions

This study presented a comprehensive approach for enhancing the recovery and enrichment of tellurium (Te) from copper tailings (CTs) through a combination of gravity separation and froth flotation techniques. Detailed mineralogical characterization using TESCAN's integrated mineral analysis (TIMA) provided critical insights into the deportment and liberation behavior of Te minerals within CT, revealing that over 90% of Te was locked within pyrite grains and predominantly occurred as fine inclusions less than 20 μm in size. This necessitated the implementation of a preconcentration step to deslime the material and improve the efficiency of subsequent flotation processes.

Gravity separation experiments using the Wilfley Table demonstrated its effectiveness in desliming CT, with notable improvements in Te recovery and enrichment. Flotation experiments on preconcentrated CT (GS-C+M) indicated that an S:L ratio of 1:10 yielded the highest recovery and enrichment for Te. The optimized flotation conditions involved using 90 g/t of sodium isopropyl xanthate (SIPX) collector and 50 g/t of glycol (OREPREP X-237) frother, achieving a maximum Te recovery of 77.43% with a corresponding grade of 3.90 ppm and an enrichment ratio of 13. TIMA studies of those same conditions revealed that 92.01% of the pyrite was recovered, showing that Te mineral recovery was optimized in the flotation concentrates, where Te was primarily found in altaite, tetradymite, and petzite, with a notable association with pyrite and quartz. Additionally, Au and Ag were predominantly recovered in the form of electrum and petzite, mainly locked with pyrite, highlighting the need for further separation after process optimization. This multi-step approach of gravity separation followed by flotation effectively concentrated Te-Au-Ag minerals. This study's findings highlight the significant potential for recovering Te from CT, contributing to the sustainable supply of this critical mineral essential for clean energy technologies, particularly cadmium telluride (CdTe) thin-film solar photovoltaics (PVs).

However, this study has some limitations. Firstly, the CT samples used were obtained from rougher flotation tailings at a single major copper producer in the USA. As a result, the applicability of the process and results may be limited to specific tailing sources, production periods, and scale. Furthermore, the study did not utilize advanced statistical or mathematical models to analyze the dataset, which could have improved optimization and prediction capabilities. The focus was solely on optimizing flotation reagent type and concentration parameters without thoroughly considering other factors, such as grind size and pulp chemistry. Additionally, an in-depth understanding of the surface chemistry and adsorption behavior of Te minerals during flotation could lead to the development of more effective and selective flotation reagents for tellurides. This would greatly enhance the recovery of Te and other valuable minerals from an increasingly complex mineralogy found in processing streams. Moreover, the study did not include hydrometallurgical procedures for Te extraction, which are essential for achieving complete recovery beyond a flotation concentrate.

To address the aforementioned limitations, future research should expand the scope of tests conducted. In addition, an optimized Te concentration should be followed by testing Te extractions through various methods, such as high-pressure acid leaching, sodium sulfide leaching, thiosulfate leaching, and thiourea leaching. This will allow for the evaluation of each method's efficiency in recovering Te from the concentrates. To achieve complete optimization, comprehensive modeling techniques should be implemented throughout the processes, enabling scalability and facilitating techno-economic analysis.

In summary, this study offers promising approaches for the sustainable recovery of Te from CT, effectively addressing both environmental and economic challenges associated with critical mineral supply. The findings highlight the importance of ongoing research and innovation in mineral processing technologies to secure the supply of essential elements for future energy solutions.

Author Contributions: Conceptualization, L.A. and J.L.C.-A.; methodology, L.A. and J.L.C.-A.; formal analysis, J.L.C.-A.; investigation, J.L.C.-A.; resources, L.A. and J.L.C.-A.; data curation, J.L.C.-A.; writing—original draft preparation, J.L.C.-A.; writing—review and editing, L.A. and J.L.C.-A.; visualization, L.A. and J.L.C.-A.; supervision, L.A.; project administration, L.A.; funding acquisition, L.A. All authors have read and agreed to the published version of the manuscript.

Funding: This research was funded by the National Renewable Energy Laboratory (NREL), USA, Award #0073551.

Data Availability Statement: Data is contained within the article.

Acknowledgments: The authors would like to acknowledge their industry partners and the National Renewable Energy Laboratory (NREL) for sponsoring the research. We would also like to acknowledge the technical and research staff at ActLabs, Gary Wyss from Montana Tech, and Missouri S&T for their contributions to the work. Additionally, the researchers wish to highlight the Missouri S&T Critical Minerals team, which supported this research: Mike Moats, Fardis Nakhaei, and Mulenga Chibesa. Additionally, the researchers want to acknowledge Peter Nso, Morgan Coulvern, and K. Cathrine Monyake for their time and suggestions during the experimental runs.

Conflicts of Interest: The authors declare no conflicts of interest.

References

- Hayes, S.M.; McCullough, E.A. Critical Minerals: A Review of Elemental Trends in Comprehensive Criticality Studies. *Resour. Policy* **2018**, *59*, 192–199. [CrossRef]
- Nassar, N.T.; Kim, H.; Frenzel, M.; Moats, M.S.; Hayes, S.M. Global Tellurium Supply Potential from Electrolytic Copper Refining. *Resour. Conserv. Recycl.* **2022**, *184*, 106434. [CrossRef]
- O’Sullivan, M.L.; Bordoff, J. *A Critical Minerals Policy for the United States*; Wilson Center: Washington, DC, USA, 2023.
- Government of Canada Critical Minerals. Available online: <https://www.nrcan.gc.ca/our-natural-resources/minerals-mining/critical-minerals/23414> (accessed on 21 September 2021).
- The White House Securing a Made in America Supply Chain for Critical Minerals. Available online: <https://www.whitehouse.gov/briefing-room/statements-releases/2022/02/22/fact-sheet-securing-a-made-in-america-supply-chain-for-critical-minerals/> (accessed on 9 October 2023).
- Commonwealth of Australia. *Critical Minerals Strategy—2030*; Commonwealth of Australia: Canberra, Australia, 2023.
- Nassar, N.T.; Fortier, S.M. Methodology and Technical Input for the 2021: Review and Revision of the U.S. Critical Minerals List. In *U.S. Geological Survey Open File Report*; Series Number 2021–1045; U.S. Geological Survey: Reston, VA, USA, 2021. [CrossRef]
- Islam, M.M.; Sohag, K.; Alam, M.M. Mineral Import Demand and Clean Energy Transitions in the Top Mineral-Importing Countries. *Resour. Policy* **2022**, *78*, 102893. [CrossRef]
- Parthemore, C. *Elements of Security: Mitigating the Risks of U.S. Dependence on Critical Minerals*; Center for a New American Security: Washington, DC, USA, 2011.
- Wilkinson, J.; Champagne, F.-P. *The Canadian Critical Minerals Strategy*; Government of Canada: Ottawa, ON, Canada, 2022.
- Flanagan, D.M. Selenium and Tellurium Statistics and Information. Available online: <https://www.usgs.gov/centers/national-minerals-information-center/selenium-and-tellurium-statistics-and-information> (accessed on 20 March 2024).
- Cohen, B.L. Anomalous Behavior of Tellurium Abundances. *Geochim. Cosmochim. Acta* **1984**, *48*, 203–205. [CrossRef]
- Wang, S. Tellurium, Its Resourcefulness and Recovery. *JOM* **2011**, *63*, 90–93. [CrossRef]
- Goldfarb, R.J.; Berger, B.R.; George, M.W.; Seal, R.R., II. *Tellurium*; Schulz, K.J., DeYoung John, H., Jr., Seal, R.R., II, Bradley, D.C., Eds.; NYRB: Reston, VA, USA, 2017.
- Li, Z.; Qiu, F.; Tian, Q.; Yue, X.; Zhang, T. Production and Recovery of Tellurium from Metallurgical Intermediates and Electronic Waste—A Comprehensive Review. *J. Clean. Prod.* **2022**, *366*, 132796. [CrossRef]
- Yano, R.I. Trace Element Distribution in Chalcopyrite-Bearing Porphyry and Skarn Deposits. Master’s Thesis, University of Nevada, Reno, Reno, NV, USA, 2012.
- Pals, D.W.; Spry, P.G. Telluride Mineralogy of the Low-Sulfidation Epithermal Emperor Gold Deposit, Vatukoula, Fiji. *Miner. Pet.* **2003**, *79*, 285–307. [CrossRef]
- Moats, M.S.; Alagha, L.; Awuah-Offei, K. Towards Resilient and Sustainable Supply of Critical Elements from the Copper Supply Chain: A Review. *J. Clean. Prod.* **2021**, *307*, 127207. [CrossRef]
- Mao, J.; Wang, Y.; Ding, T.; Chen, Y.; Wei, J.; Yin, J. Dashuigou Tellurium Deposit in Sichuan Province, China: S, C, O, and H Isotope Data and Their Implications on Hydrothermal Mineralization. *Resour. Geol.* **2002**, *52*, 15–23. [CrossRef]
- Yin, J.; Xiang, S.; Yang, K.; Shi, H.; Yin, Y. Review of Tellurium Resources in the World and in China. *Adv. Soc. Sci. Manag.* **2023**, *1*, 41–51.
- Sindeeva, N.D. *Mineralogy and Types of Deposits of Selenium and Tellurium*; Ingerson, E., Ed.; Interscience Publisher: New York, NY, USA, 1964.
- Warr, L.N. IMA–CNMNC Approved Mineral Symbols. *Miner. Mag.* **2021**, *85*, 291–320. [CrossRef]

23. Azevedo, M.; Baczynska, M.; Bingoto, P.; Callaway, G.; Hoffman, K. *The Raw-Materials Challenge: How the Metals and Mining Sector Will Be at the Core of Enabling the Energy Transition*; McKinsey & Company: New York, NY, USA, 2022.
24. Vartiainen, E.; Masson, G.; Breyer, C.; Moser, D.; Román Medina, E. Impact of Weighted Average Cost of Capital, Capital Expenditure, and Other Parameters on Future Utility-Scale PV Levelised Cost of Electricity. *Prog. Photovolt. Res. Appl.* **2020**, *28*, 439–453. [CrossRef]
25. Bauer, D.J.; Nguyen, R.T.; Smith, B.J. *Critical Materials*; U.S. Department of Energy: Washington, DC, USA, 2023.
26. Corchado-Albelo, J.L.; Locmelis, M.; Moats, M.S.; Alagha, L. Approaches for Coprocessing Tellurides: A Critical Minerals Perspective with Emphasis on Mineralogy and Metallurgy. *Miner. Process. Extr. Metall. Rev.* **2024**, 1–21. [CrossRef]
27. Hayes, S.M.; Ramos, N.A. Surficial Geochemistry and Bioaccessibility of Tellurium in Semiarid Mine Tailings. *Environ. Chem.* **2019**, *16*, 251–265. [CrossRef]
28. Corchado-Albelo, J.; Alagha, L. Characterization of Tellurium, Gold, and Silver Minerals in Copper Porphyry Processing Streams. In Proceedings of the Minexchange SME 2023 Conference, Denver, CO, USA, 1 March 2023; p. 1.
29. van der Ent, A.; Parbhakar-Fox, A.; Erskine, P.D. Treasure from Trash: Mining Critical Metals from Waste and Unconventional Sources. *Sci. Total Environ.* **2021**, *758*, 143673. [CrossRef] [PubMed]
30. Suppes, R.; Heuss-Aßbichler, S. Resource Potential of Mine Wastes: A Conventional and Sustainable Perspective on a Case Study Tailings Mining Project. *J. Clean. Prod.* **2021**, *297*, 126446. [CrossRef]
31. Corchado-Albelo, J.L.; Alagha, L. Studies on the Enrichment Feasibility of Rare Earth-Bearing Minerals in Mine Tailings. *Minerals* **2023**, *13*, 301. [CrossRef]
32. Nakhaei, F.; Corchado-Albelo, J.; Alagha, L.; Moats, M.; Munoz-Garcia, N. Progress, Challenges, and Perspectives of Critical Elements Recovery from Sulfide Tailings. *Sep. Purif. Technol.* **2024**, 128973. [CrossRef]
33. Actlabs. Geochemistry Schedule of Services & Fees. 2023 International. 2023, pp. 9–11. Available online: <https://actlabs.com/wp-content/uploads/2023/03/Actlabs-Schedule-of-Services-CAD-2023.pdf> (accessed on 11 October 2023).
34. Hrstka, T.; Gottlieb, P.; Skála, R.; Breiter, K.; Motl, D. Automated Mineralogy and Petrology—Applications of TESCAN Integrated Mineral Analyzer (TIMA). *J. Geosci.* **2018**, *63*, 47–63. [CrossRef]
35. Amosah, M.E.; Yvon, M.; Zhou, J.; Galvin, K.P. The Role of Enhanced Desliming and Gravity Separation as a Precursor to Flotation in the Upgrading of Cassiterite from Tailings. *Miner. Eng.* **2024**, *208*, 108581. [CrossRef]
36. Guest, R.N.; Svobodat, J.; Venter, W.J.C. The Use of Gravity and Magnetic Separation to Recover Copper and Lead from Tsumeb Flotation Tailings. *J. S. Afr. Inst. Min. Metall.* **1988**, *88*, 21–26.
37. Trethewey, W.D. *The Utilization of Copper-Nickel Tailing-A Literature Survey-Prep Ared for the Minnesota State Planning Agency and the Copper-Nickel Regional Study*; Minnesota Legislature: Minneapolis, MN, USA, 1977.
38. Jena, S.S.; Tripathy, S.K.; Mandre, N.R.; Venugopal, R.; Farrokhpay, S. Sustainable Use of Copper Resources: Beneficiation of Low-Grade Copper Ores. *Minerals* **2022**, *12*, 545. [CrossRef]
39. Jena, M.S.; Mohanty, J.K.; Sahu, P.; Venugopal, R.; Mandre, N.R. Characterization and Pre-Concentration of Low Grade PGE Ores of Boula Area, Odisha Using Gravity Concentration Methods. *Trans. Indian Inst. Met.* **2017**, *70*, 287–302. [CrossRef]
40. Strong, T.R.; Driscoll, R.L. *A Process for Reducing Rocks and Concentrating Heavy Minerals*; USGS: Reston, VI, USA, 2016.
41. Outotec. *Wilfley Concentrating Table*; Outotec: Espoo, Finland, 2017.
42. Yang, W.; Wang, G.; Wang, Q.; Dong, P.; Cao, H.; Zhang, K. Comprehensive Recovery Technology for Te, Au, and Ag from a Telluride-Type Refractory Gold Mine. *Minerals* **2019**, *9*, 597. [CrossRef]
43. IEA. *Global Critical Minerals Outlook 2024*; IEA: Paris, France, 2024.
44. Wang, C.; Harbottle, D.; Liu, Q.; Xu, Z. Current State of Fine Mineral Tailings Treatment: A Critical Review on Theory and Practice. *Miner. Eng.* **2014**, *58*, 113–131. [CrossRef]
45. Nykänen, V.P.S.; Braga, A.S.; Pinto, T.C.S.; Matai, P.H.L.S.; Lima, N.P.; Leal Filho, L.S.; Monte, M.B.M. True Flotation versus Entrainment in Reverse Cationic Flotation for the Concentration of Iron Ore at Industrial Scale. *Miner. Process. Extr. Metall. Rev.* **2020**, *41*, 1514298. [CrossRef]
46. Molatlhegi, O.; Alagha, L. Ash Depression in Fine Coal Flotation Using a Novel Polymer Aid. *Int. J. Clean Coal Energy* **2016**, *5*, 65–85. [CrossRef]
47. Hayat, M.B.; Alagha, L.; Sannan, S.M. Flotation Behavior of Complex Sulfide Ores in the Presence of Biodegradable Polymeric Depressants. *Int. J. Polym. Sci.* **2017**, *2017*, 4835842. [CrossRef]
48. Alsafasfeh, A.; Alagha, L.; Alzidaneen, A.; Nadendla, V.S.S. Optimization of Flotation Efficiency of Phosphate Minerals in Mine Tailings Using Polymeric Depressants: Experiments and Machine Learning. *Physicochem. Probl. Miner. Process.* **2022**, *54*, 150477. [CrossRef]
49. Alsafasfeh, A.; Khodakarami, M.; Alagha, L.; Moats, M.S.; Molatlhegi, O. Selective Depression of Silicates in Phosphate Flotation Using Polyacrylamide-Grafted Nanoparticles. *Miner. Eng.* **2018**, *127*, 198–207. [CrossRef]
50. Khodakarami, M.; Alagha, L. High-Performance Polymers for Separation and Purification Processes: An Overview. *Polym.-Plast. Technol. Eng.* **2017**, *56*, 2019–2042. [CrossRef]
51. Khodakarami, M.; Alagha, L.; Burnett, D.J. Probing Surface Characteristics of Rare Earth Minerals Using Contact Angle Measurements, Atomic Force Microscopy, and Inverse Gas Chromatography. *ACS Omega* **2019**, *4*, 13319–13329. [CrossRef] [PubMed]

52. Farrokhpay, S.; Ndlovu, B.; Bradshaw, D. Behavior of Talc and Mica in Copper Ore Flotation. *Appl. Clay Sci.* **2018**, *160*, 270–275. [\[CrossRef\]](#)
53. Chen, X.; Peng, Y. Managing Clay Minerals in Froth Flotation—A Critical Review. *Miner. Process. Extr. Metall. Rev.* **2018**, *39*, 289–307. [\[CrossRef\]](#)
54. Xie, L.; Wang, J.; Lu, Q.; Hu, W.; Yang, D.; Qiao, C.; Peng, X.; Peng, Q.; Wang, T.; Sun, W.; et al. Surface Interaction Mechanisms in Mineral Flotation: Fundamentals, Measurements, and Perspectives. *Adv. Colloid Interface Sci.* **2021**, *295*, 102491. [\[CrossRef\]](#) [\[PubMed\]](#)
55. Yan, D.S. Hariyasa Selective Flotation of Pyrite and Gold Tellurides. *Miner. Eng.* **1997**, *10*, 327–337. [\[CrossRef\]](#)
56. Dimou, A. The Flotation of Pyrite Using Xanthate Collectors. Master's Thesis, University of Cape Town, Cape Town, South Africa, 1986.
57. Sun, Z.; Forsling, W. The Degradation Kinetics of Ethyl-Xanthate as a Function of PH in Aqueous Solution. *Miner. Eng.* **1997**, *10*, 389–400. [\[CrossRef\]](#)
58. Mermillod-Blondin, R.; Kongolo, M.; De Donato, P.; Benzaazoua, M.; Barrès, O.; Bussière, B.; Aubertin, M. Pyrite Flotation with Xanthate under Alkaline Conditions—Application to Environmental Desulfurisation. In Proceedings of the Australasian Institute of Mining and Metallurgy Publication Series, Melbourne, Australia, 7–9 March 2005.
59. Shen, Y.; Nagaraj, D.R.; Farinato, R.; Somasundaran, P. Study of Xanthate Decomposition in Aqueous Solutions. *Miner. Eng.* **2016**, *93*, 10–15. [\[CrossRef\]](#)
60. Zhang, J.; Zhang, Y.; Richmond, W.; Wang, H.P. Processing Technologies for Gold-Telluride Ores. *Int. J. Miner. Met. Mater.* **2010**, *17*, 1–10. [\[CrossRef\]](#)
61. O'Connor, C.T.; Shackleton, N.J. Investigations into the Recovery of Platinum Group Minerals from the Platreef Ore of the Bushveld Complex of South Africa. *Platin. Met. Rev.* **2013**, *57*, 302–310. [\[CrossRef\]](#)
62. Dickinson, J.E.; Galvin, K.P. Fluidized Bed Desliming in Fine Particle Flotation—Part I. *Chem. Eng. Sci.* **2014**, *108*, 283–298. [\[CrossRef\]](#)
63. Galvin, K.P.; Dickinson, J.E. Fluidized Bed Desliming in Fine Particle Flotation—Part II: Flotation of a Model Feed. *Chem. Eng. Sci.* **2014**, *108*, 299–309. [\[CrossRef\]](#)
64. Bulatovic, S.M. *Handbook of Flotation Reagents: Chemistry, Theory and Practice*; Elsevier: Petersborough, ON, Canada, 2007; Volume 1, ISBN 0444530290.
65. Bulatovic, S.M. *Handbook of Flotation Reagents: Chemistry, Theory and Practice. [Volume 2], Flotation of Gold, PGM and Oxide Minerals*; Elsevier: Amsterdam, The Netherlands, 2010; ISBN 9780444530820.
66. Rao, S.R.; Leja, J. *Surface Chemistry of Froth Flotation: Reagents and Mechanisms*, 2nd ed.; Rao, S.R., Ed.; Kluwer Academic/Plenum Publishers: New York, NY, USA, 2004; Volume 2, ISBN 0306481790.
67. Trahar, W.J.; Senior, G.D.; Shannon, L.K. Interactions between Sulphide Minerals—The Collectorless Flotation of Pyrite. *Int. J. Miner. Process.* **1994**, *40*, 287–321. [\[CrossRef\]](#)
68. Mu, Y.; Peng, Y.; Lauten, R.A. The Depression of Pyrite in Selective Flotation by Different Reagent Systems—A Literature Review. *Miner. Eng.* **2016**, *96–97*, 143–156. [\[CrossRef\]](#)
69. Rabieh, A.; Albijanic, B.; Eksteen, J.J. A Review of the Effects of Grinding Media and Chemical Conditions on the Flotation of Pyrite in Refractory Gold Operations. *Miner. Eng.* **2016**, *94*, 21–28. [\[CrossRef\]](#)
70. Fuerstenau, M.C.; Jameson, G.J.; Yoon, R.H. *Froth Flotation: A Century of Innovation*; Society for Mining, Metallurgy, and Exploration: Englewood, CO, USA, 2009; ISBN 9780873352802.
71. Aghazadeh, S.; Mousavinezhad, S.K.; Gharabaghi, M. Chemical and Colloidal Aspects of Collectorless Flotation Behavior of Sulfide and Non-Sulfide Minerals. *Adv. Colloid. Interface Sci.* **2015**, *225*, 203–217. [\[CrossRef\]](#)
72. Moslemi, H.; Gharabaghi, M. A Review on Electrochemical Behavior of Pyrite in the Froth Flotation Process. *J. Ind. Eng. Chem.* **2017**, *47*, 1–18. [\[CrossRef\]](#)
73. Jefferson, M.; Yenial-Arslan, U.; Evans, C.; Curtis-Morar, C.; O'Donnell, R.; Parbhakar-Fox, A.; Forbes, E. Effect of Pyrite Textures and Composition on Flotation Performance: A Review. *Miner. Eng.* **2023**, *201*, 108234. [\[CrossRef\]](#)
74. Monyake, K.C.; Alagha, L. Enhanced Separation of Base Metal Sulfides in Flotation Systems Using Chitosan-Grafted-Polyacrylamides. *Sep. Purif. Technol.* **2021**, *281*, 119818. [\[CrossRef\]](#)
75. Monyake, K.; Alagha, L. Depression of Pyrite in Polymetallic Sulfide Flotation Using Chitosan-Grafted-Polyacrylamide. In Proceeding of Minexchange 2020 SME Annual Conference and Expo, Phoenix, AZ, USA, 23–26 February 2020.
76. Monyake, K.C.; Alagha, L. Evaluation of Functionalized Chitosan Polymers for Pyrite's Depression in Pb-Cu Sulfide Flotation Using Response Surface Methodology. *Min. Metall. Explor.* **2022**, *39*, 1205–1218. [\[CrossRef\]](#)
77. Monyake, K.; Han, T.; Ali, D.; Alagha, L.; Kumar, A. Experimental and Machine Learning Studies on Chitosan-Polyacrylamide Copolymers for Selective Separation of Metal Sulfides in the Froth Flotation Process. *Colloid. Interfaces* **2023**, *7*, 41. [\[CrossRef\]](#)
78. He, S.; Fornasiero, D.; Skinner, W. Correlation between Copper-Activated Pyrite Flotation and Surface Species: Effect of Pulp Oxidation Potential. *Miner. Eng.* **2005**, *18*, 1208–1213. [\[CrossRef\]](#)
79. Richardson, P.E.; Chen, Z.; Tao, D.P.; Yoon, R.H. Electrochemical Control of Pyrite Activation by Copper. In Proceedings of the Electrochemistry in Mineral and Metal Processing IV, Morelos, México, 3–7 June 1996; Woods, R., Doyle, F.M., Richardson, P., Eds.; The Electrochemical Society, Inc.: Pennington, NJ, USA, 1996; Volume 4, pp. 179–190.

80. Hicyilmaz, C.; Altun, N.E.; Ekmekci, Z.; Gokagac, G. Quantifying Hydrophobicity of Pyrite after Copper Activation and DTPI Addition under Electrochemically Controlled Conditions. *Miner. Eng.* **2004**, *17*, 879–890. [[CrossRef](#)]
81. Chandra, A.P.; Gerson, A.R. A Review of the Fundamental Studies of the Copper Activation Mechanisms for Selective Flotation of the Sulfide Minerals, Sphalerite and Pyrite. *Adv. Colloid. Interface Sci.* **2009**, *145*, 97–110. [[CrossRef](#)] [[PubMed](#)]
82. Ejtemaei, M.; Nguyen, A. V Characterisation of Sphalerite and Pyrite Surfaces Activated by Copper Sulphate. *Miner. Eng.* **2017**, *100*, 223–232. [[CrossRef](#)]
83. Merkle, R.K.W.; McKenzie, A.D. The Mining and Beneficiation of South African PGE Ores—An Overview. *Geol. Geochem. Mineral. Miner. Benef. Platin.-Group Elem.* **2002**, *54*, 793–810.
84. Vermaak, M.K.G. Fundamentals of the Flotation Behaviour of Palladium Bismuth Tellurides. Ph.D. Thesis, University of Pretoria, Pretoria, South Africa, 2005.
85. Vermaak, M.K.G.; Venter, J.A.; Pistorius, P.C. Electrochemical Studies of the Interaction of Ethyl Xanthate with Pd-Bi-Te. *SIAMM-J. S. Afr. Inst. Min. Metall.* **2004**, *104*, 661–666.
86. Vermaak, M.K.G.; Pistorius, P.C.; Venter, J.A. Electrochemical and Raman Spectroscopic Studies of the Interaction of Ethyl Xanthate with Pd-Bi-Te. *Miner. Eng.* **2005**, *18*, 575–584. [[CrossRef](#)]
87. Elvy, S.B.; Williams, P.A.; Buckley, A.N. XPS Evidence for the Incongruent Surface Oxidation of Minerals in the Pd-Te-Bi System. *Surf. Interface Anal.* **1996**, *24*, 641–646. [[CrossRef](#)]
88. Duan, J.; Fornasiero, D.; Ralston, J. Calculation of the Flotation Rate Constant of Chalcopyrite Particles in an Ore. *Int. J. Miner. Process.* **2003**, *72*, 227–237. [[CrossRef](#)]
89. Pyke, B.; Fornasiero, D.; Ralston, J. Bubble Particle Heterocoagulation under Turbulent Conditions. *J. Colloid. Interface Sci.* **2003**, *265*, 141–151. [[CrossRef](#)] [[PubMed](#)]
90. Shackleton, N.J. Surface Characterisation and Flotation Behaviour of the Platinum and Palladium Arsenide, Telluride and Sulphide Mineral Species. Ph.D. Thesis, University of Cape Town, Cape Town, South Africa, 2007.
91. Shackleton, N.J.; Malysiak, V.; O'Connor, C.T. Surface Characteristics and Flotation Behaviour of Platinum and Palladium Tellurides. *Miner. Eng.* **2007**, *20*, 1232–1245. [[CrossRef](#)]

Disclaimer/Publisher's Note: The statements, opinions and data contained in all publications are solely those of the individual author(s) and contributor(s) and not of MDPI and/or the editor(s). MDPI and/or the editor(s) disclaim responsibility for any injury to people or property resulting from any ideas, methods, instructions or products referred to in the content.